Università di Pisa

Facoltà di Scienze Matematiche, Fisiche e Naturali

Corso di Laurea Specialistica in Scienze Fisiche

Anno accademico 2009/2010

Tesi di Laurea Specialistica

Radiative Corrections to Dark Matter Indirect Signals

Relatore

Prof. Alessandro Strumia

Correlatore

Dott. Gennaro Corcella

Candidato

Filippo Sala

Abstract

The computation of the energy spectra of Standard Model particles originated from the annihilation/decay of Dark Matter is of primary importance in indirect searches for Dark Matter. We compute such spectra for a large set of DM masses and annihilation/decay channels. In doing so, we employ the Monte Carlo simulation program HERWIG, and compare our results with the same analyses done with PYTHIA, obtaining in this way an estimation of the MC errors in the fluxes. MC parton shower programs do not include electroweak radiation effects, that are relevant when the DM mass is of the order of a TeV or higher, like experiments seem to suggest. Thus we consider a model-independent inclusion of electroweak corrections in the computation of the spectra by means of a new general partonic technique, and we check it by comparing the results of its application with a full computation we perform in the specific Minimal Dark Matter model, finding a very good agreement. In this model the two natural candidates for DM are a fermionic quintuplet and a scalar eptaplet, their only annihilation channel is into gauge bosons. For the both of them we consider the three-body processes DM DM $\to WW\gamma$ and DM DM $\to WWZ$ and perform the full computation of the γ, W and Z energy spectra dN/dE. Incidentally we also find that at $\mathcal{O}(M_W/M)$, with M DM mass, the results are the same for both scalar and fermionic DM.

Contents

Chapter 1

Introduction

It is nowadays well known that luminous matter forms only a small part of that present in the universe. Compelling evidences come from astrophysics, both at galactic and at larger scales, and from cosmology. Explanations have been explored both in terms of modifications of Newtonian gravity or General Relativity and in terms of the existence of new particles; while the first possibility is becoming more and more contrived, the second one is favoured by many observations. Moreover, the existence of this new kind of matter, commonly called *Dark Matter*, is also well theoretically motivated: candidates exist in different extensions of the Standard Model of particle physics.
Then it is not surprising that, expecially in the last two decades, a great experimental effort has been made to detect Dark Matter and discover its properties. The two directions mainly explored till now are those of direct detection experiments (aiming to see the scattering of DM particles with ordinary matter) and of indirect detection ones (aiming to see anomalies in cosmic rays spectra and relating them to DM annihilations in the galaxy).
LHC will also test numerous models which provide interesting dark matter candidates.
Recently relevant results have been found in indirect detection experiments: PAMELA, a satellite for the detection of high energy charged cosmic rays, found an anomaly in the energy spectrum of positrons, in the sense that the signal is well above the expected astrophysical background. Moreover there are already other experiments in activity conducting similar studies (e.g. Fermi), and others are supposed to start in the recent future (e.g. AMS/02).
One of the main motivations of this work is the above experimental situation.

Different physics issues play important roles in expressing the fluxes of high energy particles from DM annihilations/decays, as observed in indirect detection experiments. One has to compute the "primary fluxes" and then propagate them in the galaxy, including properly all the astrophysical effects which arise (DM distribution in the galaxy, effect of magnetic fields on the propagation of charged particles...). Refining the tools

related to the computation of such fluxes is of primary importance, since it affects deeply the way results from experiments of indirect detection constrain DM model building.

In this work we concentrate on primary fluxes. First we use the Monte Carlo program HERWIG to compute them in a model-independent way: we give them for a large set of masses and annihilation/decay channels of DM particles. While this has already been done using the Monte Carlo program PYTHIA, it is the first time HERWIG is used for similar purposes, a comparison will prove then very useful for obtaining an estimation of the Monte Carlo uncertaintes on these fluxes. Having at disposal such an amount of spectra is also useful to quickly extract predictions by any DM model: it suffices to compute all the branching ratios of DM in various Standard Model particles, and then use these BR as weights to linearly sum the alreday propagated fluxes.

In the second part of this thesis, we work in a specific scenario called "Minimal Dark Matter". The two cases of main interest are those where Dark Matter is a fermionic quintuplet or a scalar eptaplet, since DM is automatically stable; in both of them DM annihilates into gauge bosons. The situation we examine is quite general: it arises, for instance, in a region of the Minimal Supersymmetric Standard Model parameter space (we remember that the Lightest Supersymmetric Particle is a natural candidate for Dark Matter). In both cases, we consider the three body processes DM DM $\to WW\gamma$ and DM DM $\to WWZ$ and we perform a full computation of the γ, W and Z energy spectra dN/dE, approximating $M_Z \simeq M_W$. Since the expressions obtained are rather lenghty, we give them only at first order in $\epsilon = M_W/M \ll 1$, where M is the DM mass. The approximate result for the γ is the only one already computed in literature (for fermionic DM in a MSSM context), and it agrees with ours.
This computation is useful even in the more general context of electroweak corrections to DM primary fluxes. Their impact has been understood and sistematically studied only very recently, this work being a part of that study. Electroweak corrections bring significant effects when the mass of DM particles is larger than the electroweak scale (fact suggested by indirect detection experiments): soft electroweak gauge bosons are copiously radiated, opening new channels in the final states which otherwise would be forbidden if such corrections were neglected. All stable particles are therefore present in the final spectrum, independently of the primary channel of DM annihilation/decay. Moreover the total energy gets distributed among a large number of lower energy particles, thus enhancing the signal in the lower energy region (say, (10 - 100) GeV), that is measured by present-day experiments, like PAMELA.
Electroweak corrections have not yet been implemented in any Monte Carlo parton shower code, however they can be included in the computation of the spectra to fixed order (in the coupling constant), in a model independent way. This can be done through usual partonic techniques or through their generalization to massive partons, which of course

yields much better results. An important check of the correct inclusion of EW corrections is given by a comparison with the exact result we computed in tha specific MDM scenario: the agreement we find is very good, the above generalization playing a key role in that.

The exposition could consist only of these two topics, however this work is a thesis and it's not addressed to specialists of the field. This is why, before presenting and discussing the above results, we give a general treatment of the main issues regarding dark matter, such as evidence for its existence, its properties, and the current experimental and theoretical situation. With the same spirit, we also devote a few pages in exposing the physics lying behind the simulation of QCD radiation by means of shower Monte Carlo programs. In this preliminary part, the logic will be that of presenting results in a coherent and synthetic fashion, trying to never omit experimental and/or theoretical motivations for them.

The exposition is organised as follows: in Chapter 2 we give the observational evidences for the existence of Dark Matter, from galaxy up to cosmological scales, and we derive the properties of DM which such observations imply; in Chapter 3 we concentrate on the current experimental situation, both for direct and indirect detection, and again we explain its consequences on DM properties; in Chapter 4 we build the parton shower algorithm which is at the basis of the Monte Carlo programs we will use, and we explain the principles of how they work. The reader already familiar with these topics can jump directly to Chapter 5, where we give the energy spectra obtained using HERWIG for a big sample of DM masses and annihilation/decay channels, and where we compare them with the same ones obtained with PYTHIA. Chapter 6 is devoted to three body processes in the MDM scenario: first we give the expressions obtained by a full computation, then, after summarizing the main features of electroweak corrections to DM primary fluxes, we check them against our exact results. In Chapter 7 we conclude summing up the main results of this work and giving some of their possible prospectives.

Chapter 2

Astrophysical and Cosmological aspects of Dark Matter

In the past, whenever an anomaly in the motion of an astrophysical object was observed, two roads used to be explored: relating the anomaly to some other object which hadn't yet been seen, or modifying the laws of gravitation. The first case contains for example the discovery in 1846 of Neptune, whose existence was earlier conjectured to explain the anomalous motion of Uranus; on the contrary an analogous attempt for the deviations in the motion of Mercury failed, and the problem was solved later by Einstein's theory of General Relativity.
Today we find ourselves in a conceptually similar situation, observing anomalies on large astrophysical scales, and again both types of solution have been analyzed.
A few theories modifying the laws of gravitation have been proposed (e.g. MOND theories [3]), but usually they explained only the specific anomalies they were introduced for, while facing problems with other kinds of observations; so we won't pay them attention any more in this work.
The most widely accepted explanation is instead in terms of the existence of a new kind of "dark" matter, as its gravitational effects are able to explain many indipendent anomalous observations. It is dark in the sense that it doesn't interact directly with electromagnetic radiation and so it has never been seen before, at least by means of usual techniques.

2.1 Evidence

The first significative hint that a new kind of unobserved matter should exist came in 1933, when Zwicky applied the virial theorem to the Coma cluster of galaxies, finding out that it should have been completely dominated by non-visible matter [4]. Then a latence period of 40 years followed, interrupted by the beginning of a systematic evidence for Dark Matter both from single galaxies and from galaxy clusters. Since then, physicists

started to look seriously at the hypothesis of Dark Matter, and it turned out that it was suggested even by other observations.

2.1.1 Astrophysical evidence

From an astrophysical point of view, evidences are present both on galactic scale and on galaxy cluster scales, and come basically from *dynamical analyses* of structures, from the study of *gravitational lensing* and from *X-ray emission of hot gases*. With dynamical analyses we intend the study of the motion of luminous objects, which trace the gravitational field they are immersed in. These objects are studied by means of the electromagnetic radiation they emit, they could be stars, galaxies, clouds of cold gas and so on. Gravitational lensing is the deviation of the motion of light in a region of space which is curved by the presence of some mass; studying the deviation from straight lines allows to detemine the mass in the region. Finally a hot gas at hydrostatic equilibrium has an X-ray emission constant on equipotential surfaces: by measuring it one obtains the shape of the total gravitational potential.
The correspondence of measurements made by the use of these independent techniques has convinced almost all astrophysicists that dark matter actually exists as a major component of the universe.
We will be interested here only in the main ideas lying behind those evidences, thus our exposition will be in some point rather informal. A more detailed astrophysical discussion, though really interesting, goes beyond the purposes of this thesis; the interested reader is referred to Roncadelli's book [5].

On galactic scales the first evidence comes from observations of rotation curves of spiral galaxies, namely the distributions of angular velocities v of stars and gases versus their distances from the galactic center r. From a simple calculation one would expect a profile of the type

$$v(r) = \sqrt{\frac{GM(r)}{r}},$$

where G is the Newton constant and $M(r)$ is the mass contained in the radius r, which, after introducing $\rho(r)$ for the mass density profile, takes the form $M(r) = 4\pi \int_0^{+\infty} \rho(r) r^2 dr$. If one assumes all the matter in a galaxy to be luminous, velocity should fall as $1/\sqrt{r}$ outside the visible radius R_{opt} (tipical values for R_{opt} are of the order of 10 Kpc); this should be true even inside the galaxy, or at least in its outer regions, since one expects $M(r)$ to be constant in r (i.e. $\rho(r) \propto 1/r^3$). Observations give instead evidence for a flat behaviour in r, as can be seen from figure (2.1).
That suggests that an halo of dark matter exists, with $\rho(r) \propto 1/r^2$ and $M(r) \propto r$, extending to distances bigger than R_{opt}.

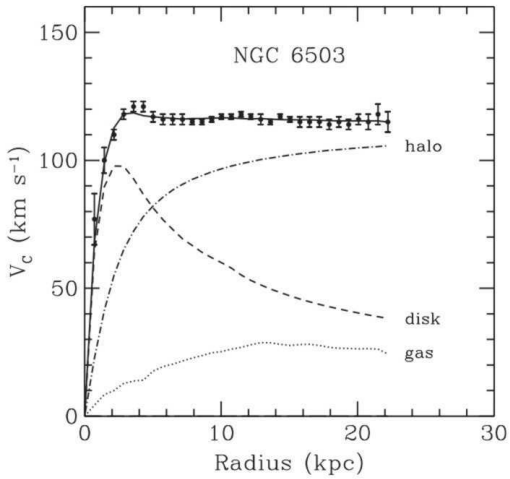

Figure 2.1: Rotation curve of NGC 6503. The dotted, dashed and dash-dotted lines are the contributions of gas, disk and dark matter respectively. Figure taken from [1].

Measures of rotation curves come both from direct observations of the motion of visible matter in the galaxy (through Doppler shifts in its electromagnetic spectrum) and from the shift of the characteristic emission line (in the radio band) of cold nubes of H_2, present even at distances larger than R_{opt}. The fact that these two measurements are independent leads almost unequivocally to the conclusion that spiral galaxies are immersed in a dark halo, and that it extends far away the luminous region.
A really important role in separating the visible and dark contribution to rotation curves has been played by Low Surface Brightness galaxies (LSB), since they're almost completely dominated by Dark Matter (supposed to make around the 95% of their mass).
For elliptical galaxies measurements of velocity are more difficult, since the stars they contain do not have an ordered motion; anyway even for them evidence for a huge presence of dark matter has been found. Here the main technique used for making the measure has been the statistical study of the stars velocity dispersion, but this dynamical analysis is not as accurate as the one performed for spiral galaxies.
Other important evidences at this scale, present for both types of galaxies, are the effect of gravitational lensing (both strong and weak) they have on more distant galaxies and the study of the X-ray emissions of hot gases. The last one becomes really important for elliptical galaxies, since for them it is this technique that furnishes the most precise indications on the amount of unseen matter.

On galaxy cluster scales, the method Zwicky used in the thirties to infer that the Coma cluster should have been dominated by dark matter has been applied to a lot of other clusters, finding sistematically analogous results. It consists basically in measuring the average velocity dispersion of galaxies $\langle v \rangle$, then deducing the average value of the gravitational potential V by means of the virial theorem $\langle T \rangle = -\langle V \rangle$, where T is the to-

tal kinetic energy of the system. The high values found for V demand an amount of dark mass that, in some cases, could exceed the visible one even by two orders of magnitude. Again, these observations are in agreement with those made by the study of weak gravitational lensing effects and X-ray emission by hot gases in the cluster.
In August 2006 the Bullet cluster provided what it is thought to be, according to many astrophysicists, the best evidence to date for existence of dark matter. The Bullet cluster is a system of two colliding clusters of galaxies for which a spatial offset of the centre of the total mass from the center of the visible mass peaks has been observed. The importance of this observation is that, with a statistical significance of 8 σ, the offset cannot be explained with an alteration of the gravitational force law, while the presence of Dark Matter can account for the displacement [6]. More recently, other galaxy clusters collisions have shown an analogous displacement.

The above discussion on astrophysical evidence showed that the existence of a large amount of non-luminous matter is required, but apparently it didn't provide any information whether it should be baryonic or not. Constituents of non-luminous baryonic matter are astronomical objects with a very low absolute luminosity, which thus evade direct observation, for example white dwarves, brown dwarves, neutron stars, black holes and cold gas clouds. Could dark matter haloes of galaxies be formed by these non-luminous baryonic objects? Astrophysics exclude the majority of them, since otherwise there would be an excessive presence of heavy elements in the haloes, and that would lead to an unobserved electromagnetic emission. The more convincing astrophysical evidence that Dark Matter is non-baryonic is however the Bullet Cluster, since, if Dark Matter were baryonic, it would interact more in the collision and not give rise to the observed displacement between the center of the total mass and the center of the visible mass. Anyway it is cosmology which provides the clearest indication that the new non luminous matter is composed, at least in its major part, by non-baryonic matter.

2.1.2 Cosmological evidence

Cosmology strongly requires the existence of a new type of non-baryonic matter: we summarize how in the following, and we refer to Dodelson's book [7] for a complete treatment.
According to the Big Bang model, almost the totality of light elements present today in the universe, such as H, ^{2}H, ^{3}He, ^{4}He, ^{7}Li, formed during its first minutes of life. To be in agreement with the abundancies observed today, big bang nucleosynthesis (BBN) requires a contribution of barionic matter to the cosmic density of $\Omega_B \simeq 0.04 - 0.05$.
More complete information can be obtained with the study of the spectrum of Cosmic

Microwave Background (CMB). It emerges that the total cosmic density must be 1,

$$\Omega = 1$$

and that

$$\Omega_B \simeq 0.045,$$

in agreement with BBN prediction.
The study of supernovae red shift put in evidence that today the expansion of the universe is accelerated. If the universe contained only matter one would expect, as a consequence of gravitational attraction, that its expansion would decelerate. The most widely accepted explanation of this acceleration is the hypothesis that the universe is dominated by a new type of energy, commonly called dark energy, possessing a negative pression. Again by the study of CMB it is possible to infer its contribution Ω_Λ to the cosmic density in terms of the contribution of matter Ω_M, finding

$$\Omega_\Lambda \simeq 1.40\,\Omega_M + 0.35.$$

Cosmology also tells us that the contribution of radiation to the total cosmic density Ω is today negligible (order of 10^{-3}), so we can write $\Omega = \Omega_M + \Omega_\Lambda \simeq 2.40\,\Omega_M + 0.35$ and obtain that

$$\Omega_M \simeq 0.27. \tag{2.1}$$

It has turned out that baryonic matter forms less than the 20% of matter contained in the universe, thus the existence of a new type of non-baryonic matter is required. The Dark Matter we found evidence for previously can even account for this cosmological observation.

Now that we've seen that the existence of Dark Matter explains a huge quantity of very different observations, we're ready to describe how these observations quantitavely determine its properties.

2.2 Properties

The same techniques we used to deduce evidence for the existence of Dark Matter are fundamental in providing many measurements and quantitative predictions of the properties which it should have. As in the previous subsection, we proceed from galaxy up to cosmological scales.

2.2.1 Dark Matter distribution in the Galaxy

Indications of the total mass M_{tot} of matter (including unseen matter) present in galactic haloes come from both the statistical study of the orbits of satellite galaxies and from weak lensing, this two kind of observations suggest, for spiral galaxies, a typical value of approximately (see [5])

$$M_{tot} \simeq 2 \cdot 10^{12} M_{\odot}, \tag{2.2}$$

where $M_{\odot}$ is the mass of the sun. This result is really important, since the two techniques are based on completely different hypothesis. Thay also agree on the fact that the quantity of Dark Matter present in the visible region of the galaxy is substantially equal to that of visible matter.
By the same methods, the radious to which the Dark Matter halo extend can be determined, again the two techniques for measuring it agree, yielding typically

$$R_{DM} \simeq 200\, kpc \tag{2.3}$$

It is notable that an inferior limit of approximately 100 kpc for R_{DM} has been obtained via the observation of X-ray emission of hot gases. For some kind of elliptical galaxies values of R_{DM} reaching 400 kpc have also been found.
In obtaining some of the above results, as in the discussion of the preceding subsection, the approximation of a spherical symmetry of the galactic halo has been implicitly used. This assumption nonetheless finds strong observational support, for example by the measurement of (spiral) galaxy disk thickness as a function of the distance from the centre of the galaxy. This quantity is the result of the competiton of the gradient of the pressure of the gas and of the gravitational field the disk is immerse in, so it provides a good indication of the global shape of the dark matter halo. In this way it has been found that their shape is that of ellipses with a very small flattening, which justifies the approximation of spherical symmetry. The same result has been obtained independently with the study of X-ray emission by hot gases.
A lot of work has been done to determine the spherical shape of dark matter mass density $\rho(r)$ in the halo. A simplified analysis of rotation curves yielded a behaviour like $\rho(r) \approx 1/r^2$, at least for large distances from the galactic center. Much more precise results can be obtained by means of N-body simulations for large-scale structure formation. Anyway we still don't have a really satisfactory knowledge of large-scale structures, since many physical processes take part in their evolution, starting from primordial density fluctuations, recombination, radiative cooling down to gas dynamics and other astrophysical effects. Moreover, even at observational level, many complications arise when we look for confirmations of theoretical models.

This lack of understanding is reflected in the fact that results of simulations made by different groups are far from finding an agreement. A parametrization for the mass density profile suggested by various works is

$$\rho(r) = \frac{\rho_0}{(r/R)^\gamma \left[1 + (r/R)^\alpha\right]^{\frac{\beta-\gamma}{\alpha}}}, \tag{2.4}$$

where ρ_0 and R are parameters to be fit to observations, and thus depend on the galaxy we're studying, and α, β and γ are predicted by simulations. Different groups have found different values for them, in Table 2.1 we report as an example those obtained by Navarro, Frenk and White (NFW) [8], by Moore [9] and using the Isothermal model [10, 11].
Recently other kinds of parametrization (e.g. the Einasto profile [12, 13]) have emerged as better fits to numerical simulations.

	α	β	γ
NFW	1.0	3.0	1.0
Moore	1.5	3.0	1.5
Iso	2.0	2.0	0

Table 2.1: Parameters of some widely used profile models for dark matter density in galaxies.

It is worth to spend a few words on the behaviour of the mass density profile near the center of galaxies, since the presence of a more dense core can be crucial for indirect detection experiments. While for Isothermal models the profile in this zone is rather shallow (as can be seen from the parameters in Table 2.1), the majority of other models provides for the presence of a cusp there, though without an agreement on its slope (see for example the paremeters of NFW and Moore models). Another complication arises if a super massive black hole (SMBH) exists in the center of the galaxy, in such a case it has been found that the process of adiabatic accretion of dark matter on it would produce a "spike" in the dark matter density profile.
Given the uncertaintes regarding observed and simulated halo profiles, and their consequences on the observed dark matter annihilation fluxes (expecially from the galactic center), the approach commonly used in indirect detection literature is that of computing those fluxes for a large set of halo profiles, without making a specific choice.
The study of the Milky Way has proved very useful for the above issues, due to the wide range of observational data available. For example there is quite an agreement on the presence of a SMBH in its center, though its consequences on the halo profile are not yet clear. The study of our galaxy has also been really important for detecting MACHO (Massive Astronomical Compact Halo Objects) and for excluding them as candidates to (barionic) dark matter. Techniques similar to those used in this case, such as gravitational lensing, could hopefully shed light on properties of Dark Matter "subhaloes" (i.e. more

dense regions in the halo profile), whose existence is predicted by most numerical simulations. While there is observational agreement on their existence, current experiments seem to find their abundance to be noticeably lower than what predicted by simulations. These issues are of extreme importance for interpreting the resuts of indirect detection experiments, since the presence of more dense substructures could affect the propagation of DM annihilation products in the galaxy, enhancing the observed fluxes up to one or two orders of magnitude.

2.2.2 Dark Matter in the Solar System

Studying the Milky Way one can also measure properties of the DM in the Solar System, such as the density ρ_0 and the average quadratic velocity $\bar{v}$, which are fundamental to the prospects for both direct and indirect detection. The typical value found for the velocity is

$$\bar{v} \simeq 270\, km/s,$$

while for the local density there isn't such an agreement, as one could expect from the lack of understanding of dark matter halo profiles. Anyway an acceptable range has been identified ([15],[16]) to be

$$\rho_0 \simeq 0.3 \pm 0.1 \text{ GeV}/cm^3,$$

and that is the one mostly used in literature (see e.g. [1], [2], [49]).

2.2.3 Dark Matter at greater scales and conclusions

Let us now discuss the properties of DM at greater scales.
The first question we pose ourselves is if all the amount of DM in galaxy clusters come from the contribution of single galaxies, or if there is a non-negligible quantity of diffused DM. The question is stricly related to the formation mechanism of cosmic structures. In fact, if the aggregation process were *top-down* (i.e. clusters form earlier, galaxies later), it would be natural to imagine a large amount of DM diffused in the clusters; on the contrary, if the scheme is *bottom-up*, one will expect to find a really small quantity of diffused DM. Numerical simulations of cosmic structures formation have clarified that the correct mechanism is the second one, so almost all the DM present in clusters should be the sum of the contributions of the single galaxies. Unfortunately these two quantities (DM in single galaxies and DM in the whole cluster) are known with a very low precision, anyway till now observations have always been in agreement with what we expect from numerical simulations. Moreover, the lack of luminous matter diffused in the clusters confirms that the cosmic structures actually formed according to a bottom-up mechanism.

There is another way of finding evidence that most of the DM in clusters is the one concentrated in single galaxies. Since the content in Dark Matter of single galaxies is a known quantity, we can then estimate what would be the content in Dark Matter of the entire universe if only galaxies contributed to it. We express this quantity as a cosmic density $\Omega_{DM,G}$. With this procedure, we find

$$\Omega_{DM,G} \simeq 0.20 - 0.30,$$

which is comparable with the more precise result (2.1) obtained from cosmology: that excludes the existence of a great amount of dark matter diffused in and among the clusters.

The above discussion on cosmic structures formation gives evidence for another very important property of DM, that is the fact of being *cold*. For cold we intend that DM had to be non relativistic when it decoupled[1] from the other constituents of the universe during cosmic expansion. That can generally be expressed with the condition

$$M \gg T,$$

where T is the temperature of the universe during matter domination and structure formation, and M is the Dark Matter mass.
This requirement finds a justification in the fact that a highly energetic Dark Matter is not in agreement with a bottom-up mechanism for cosmic structures formation. In fact, if it were highly energetic it would slow down the formation of these structures, and today we would observe a different distribution of matter in the universe. For similar reasons, Dark Matter must be a so-called WIMP (weak interacting massive particle), in the sense that high cross sections for its interaction with ordinary matter are excluded. We will be more specific on the sense of the term WIMP and give quantitative details on this issue when speaking of direct detection experiments in the next Chapter.

From cosmology one can extract another important information about DM, that is an extimate of freeze-out $\langle \sigma_A v \rangle$, the thermal average of its total annihilation cross section to all possible channels multiplied by velocity. This can be done assuming Dark Matter is the thermal relic of a particle and using the Boltzmann equation for the particle number density n evolution, which leads to

$$\frac{dn}{dt} + 3Hn = -\langle \sigma_A v \rangle (n^2 - n_{eq}^2), \tag{2.5}$$

where H is the Hubble constant and n_{eq} is the value of n at thermal equilibrium. It

[1] A particle species in the early universe has to interact sufficiently or it will fall out of thermodinamic equilibrium, becoming a so-called *thermal relic*. More precisely, when its interaction rate drops below the expansion rate of the universe, the equilibrium can no longer be mantained and the particle is said to be *docoupled*: then its properties now contain information about the universe at that time.

can be shown that (see for example [1] and [2]), with reasonable approximations, this equation turns into an expression of Ω_{DM} as a function of $\langle \sigma_A v \rangle$: using the measured value (2.1) for Ω_{DM} one can finally estimate

$$\langle \sigma_A v \rangle \approx 10^{-26} cm^3/s. \tag{2.6}$$

This is the typical value of a TeVmass particle.
We are now ready to state what the first properties of Dark Matter as a particle are:

- to be dark, it should have negligible interactions with the photon;
- to be cold, it can't consist of neutrinos, since they do not satisfy the condition $M \gg T$. Moreover they're even too light to explain the observed Ω_{DM};
- it cannot be lighter than a few keV, otherwise it would not be cold. For a more detailed analysis on this lower bound on DM mass, see for example [17] and [18].
- today it should hold $\langle \sigma_A v \rangle \approx 10^{-26} cm^3/s$, since perturbative quantum field theory predicts $\langle \sigma_A v \rangle \simeq a + b\, v^2 + \mathcal{O}(v^4)$, and the average velocity of DM has fallen from $\langle v \rangle \simeq 0.2$ at freeze-out to $\langle v \rangle \simeq 10^{-3}$ now.

The discussion of various experiments in the next section will complete and refine these properties.

Chapter 3

Experimental situation

Many experiments have searched and are currently searching for a signal of particle Dark Matter. They can be schematically classified in three groups, according to the presence of DM only in the final state (collider experiments), both in the initial and in the final state (direct detection experiments), and only in the initial state (indirect detection experiments).

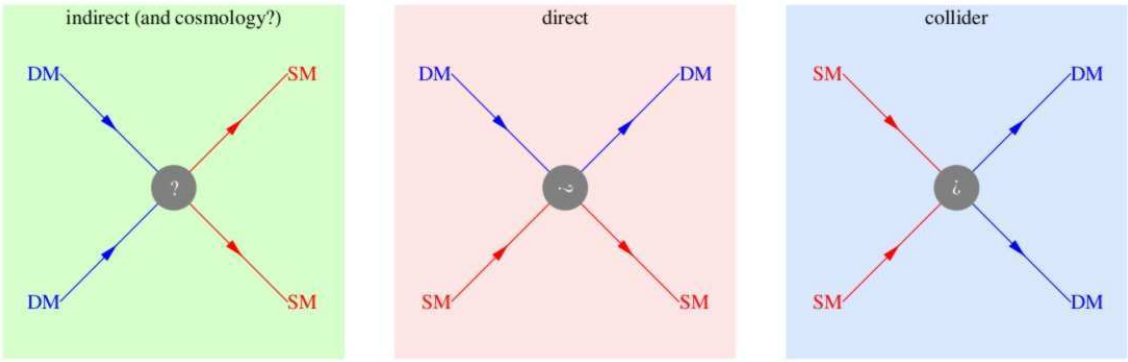

Figure 3.1: Figure taken from [22].

Producing Dark Matter in a particle accelerator would be ideal, since we would have complete control on the initial state and the experiments could be repeatable. The expected signature should be some kind of missing energy, since DM interacts very weakly with ordinary matter, and thus with detectors. Anyway, till now no evidence for it has been found, the LHC will go further in the search and test many models that provide DM candidates.
On the contrary, possible signals of Dark Matter recently came from both direct and indirect detection experiments. However many controversies are still present in their interpretation, and in some cases even in their results. That enforces the importance of working on complementary techniques in Dark Matter searches and of seeking links

between direct and indirect detection.
So, even if this work inserts itself in the context of indirect detection experiments, it is useful before to have a quick overview of the direct detection experiments situation.

3.1 Direct detection experiments

The basic idea lying behind direct detection experiments is very simple: the galaxy is filled by Dark Matter, as the Earth moves in the galaxy it will be constantly crossed by these particles, making it possible to look for their interactions with matter.
Devices built for this purpose search for the effects of scattering of DM on the material, of course they will profit by a large mass with which to receive signals, and by a long operational period. To get an idea of what their characteristics should be we summarize here the main issues of the events they look for.
First, an upper bound for the energy E which a WIMP would deposit in the apparatus is given by

$$E = \frac{1}{2} m \bar{v}^2 \simeq 40\,\mathrm{keV},$$

where we assumed the mass m of the DM to be around 100 GeV and its velocity to the value of $\bar{v} \simeq 270\,km/s$ given in the precedent chapter. A more precise expression for the energy recoil of a WIMP scattering off a nucleus of mass M will depend on the ratio μ^2/M, where μ is the reduced mass of the system WIMP-nucleus: then a higher mass of the DM would not increase the energy deposit in the apparatus. Since natural radioactivity generally emits at energies of the order of 1 MeV, a direct detection device should be radioactively clean, otherwise a keV increase in energy would be nearly impossible to find.
The kind of scattering processes considered can be classified by two features: elastic or inelastic, and spin-dependent or spin-independent.

- *Elastic scattering* is simply the interaction of the WIMP with the nucleus as a whole, causing it to recoil. Current experiments can detect recoils of energy as low as 1-10 keV, therefore they are potentially sensitive to this kind of scattering.
  In *inelastic scattering*, the WIMP interacts with orbital electrons exciting them or ionizing the target. Otherwise the WIMP can interact with the target nuclei leaving it in an excited state, then a small recoil followed by the emission of a photon is expected. However inelastic cross sections with the nuclei are generally smaller than the elastic ones.

- *Spin-dependent* scatterings come from "axial-vector" interaction terms in the La-

grangian, they result in the coupling of the WIMP's and the Nucleon's spins and are proportional to $J(J+1)$, where J is the nucleon spin. Since they do not depend on the number of nucleons, little is gained by using heavier target nuclei.
Spin-independent scatterings come from "scalar" interaction terms in the Lagrangian and are proportional to A^2, A being nucleon number. Thus, they have the advantage of higher cross sections with larger nuclei, and typically dominate over spin-dependent scatterings in current experiments which use heavy atoms as targets. See [1, Appendix C] for details.

Due to the different kind of events a WIMP-nucleon scattering can lead to, experiments have at disposal different detection techniques. They can measure the vibrations in the crystal lattice of the detector, which results in a little rise in temperature, they can search for ionization events by applying a small electric field in the detector to "push" the electron to a wall where it can be registered, and they can use scintillation, that is they gather photons emitted by excited atoms or nucleons.
To help discarding background events, a detector is usually set up to sense two of these WIMP signals, moreover other specific techniques for this purpose can vary from experiment to experiment. Other aspects in which they differ are for example the material the detector is made of (e.g. the CDMS-II collaboration employs cooled Ge and Si detectors, the ZEPLIN and the XENON collaborations liquid Xe...) and its mass (the heaviest detector being the one of the DAMA collaboration, with a mass of roughly 250 Kg, compared to masses of $\mathcal{O}(1)$ kg of the majority of other experiments). Such a use of various techniques and technologies is fundamental to vary the systematic error from experiment to experiment, better allowing for a critical assessment of a positive signal; that makes direct detection experiments a really promising way to detect particle Dark Matter.

Currently more than 20 experiments of this kind are either operating or in development. Till now there isn't an agreement on a positive signal, even if DAMA [19] and, more recently, CoGeNT [20] and CDMS [21], claim to have observed events due to DM scatterings off their detectors. The conciliation of these three results among themselves, and their coherence with other experiments negative results are still a source of debate in the scientific community.
In Figure 3.2 we present a plot with the exclusion curves given by various experiments, the "DAMA anomaly" is also shown.
Detectors made (or partly made) of materials with non-zero spin nuclei, such the ones used by the CDMS and the PICASSO collaborations, have provided upper limits even on spin-dependent cross sections.

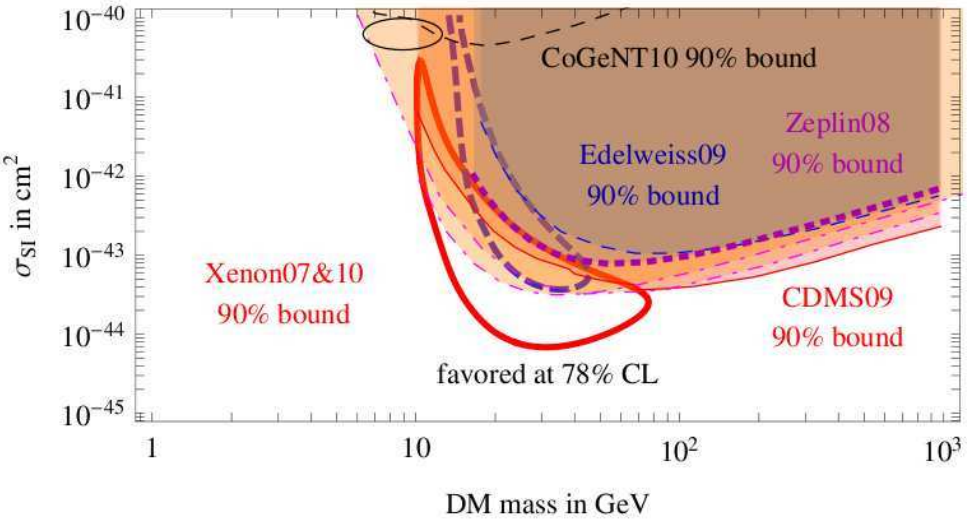

Figure 3.2: Spin independent cross section versus WIMP mass with exclusion curves. The thick red curve encloses the region favored at 78% confidence level by experiments. The black ellipse on the top is the DAMA claimed discovery region. Figure taken from [22]

3.2 Indirect detection experiments

A potential signal from Dark Matter are the products of its self-annihilations and/or decays.

It is an *indirect* signal, since it doesn't allow to actually detect the WIMPs themselves.

A similar signal could come from regions where high densities of Dark Matter are expected to be present, such as the sun or the galactic center. This statement holds expecially for DM annihilation, since the annihilation rate is proportional to the square of the DM density, $\Gamma_A \propto \rho_{DM}^2$, while for the decay rate $\Gamma_D \propto \rho_{DM}$. Keeping this in mind, in the following we will refer to DM annihilation implying even DM decay, except when explicitely specified.

Dark Matter annihilations would yield to an excess of particles in cosmic rays, with respect to those expected taking into account only ordinary astrophysical sources. Indirect detection experiments then aim to detect cosmic rays particles (mainly electrons and positrons, protons and antiprotons, deuterium, photons and neutrinos) and to measure their properties, such energy spectra and direction. Because of high low energy astrophysical backgrounds, the regions where one hopes to see a DM indirect signal are those of high energy cosmic rays (i.e. from $\mathcal{O}(10)$ GeV).

3.2.1 Antimatter

Antimatter can be an excellent signal of DM annihilation, because it is relatively rare cosmically and many of the astrophysical processes which produce it are well understood. However, unlike gamma-rays and neutrinos it is charged, and so its trajectory in galactic and extragalactic space is deviated by magnetic fields; moreover it is affected by processes as inverse Compton scattering and the emission of synchrothron radiation. So, when we detect it, it contains no information of where it came from, hardly allowing to test if Dark Matter is present only locally or everywhere in the Milky Way; also, the various physics issues coming into play in antimatter propagation complicate its treatment. Then no definitive deduction on Dark Matter can be made from these data, unless they're analyzed together with the results of other different observations: we will see what conclusions such an analyses leads to at the end of the chapter.
Experiments looking for antimatter must be located near the top or outside the Earth atmosphere, otherwise particle showers from other cosmic rays produce too large backgrounds. Experiments of this type are for example the balloon experiments HEAT, BESS and CAPRICE, which measured the spectra of positrons and antiprotons up to energies of 30-40 GeV, and the most recent satellite PAMELA, which reached energies of more than 100 GeV and, in 2008, observed a clear excess in the "positron fraction" $e^+/(e^+ + e^-)$ [23], that is the ratio of the positron flux to the sum of the positron and electron fluxes (see Figure 3.3 for a comparison of the data with the expected astrophysical background). Explications of this excess in terms of a not-yet-seen astrophysical source, like a nearby pulsar, have been tried [24]. Anyway till now no such an object has been observed, leaving the excess without a definitive explaination.
PAMELA also measured the energy spectra of the "antiproton fraction", finding no excess in this case; data for the neat positron and antiproton fluxes are expected for autumn 2010. AMS-02, another similar experiment with improved features, will be launched in February 2011.

3.2.2 Gamma-rays

Gamma-rays have the good aspect of a much simpler propagation in the galaxy, and the good and the bad aspect at the same time of being directional. It is good because we can infer the direction of their source, and then, for the prospect of DM, we can point our observations to zones where we expect it to have higher concentrations, as the sun or the galactic center. It is bad because the fluxes are highly dependent on the DM halo distribution which, expecially in these zones, have a lot of uncertaintes; however these observations can provide a test of its dependence on astrophysical parameters.
Gamma-rays direct observation can only be made from space. In fact, in the energy range

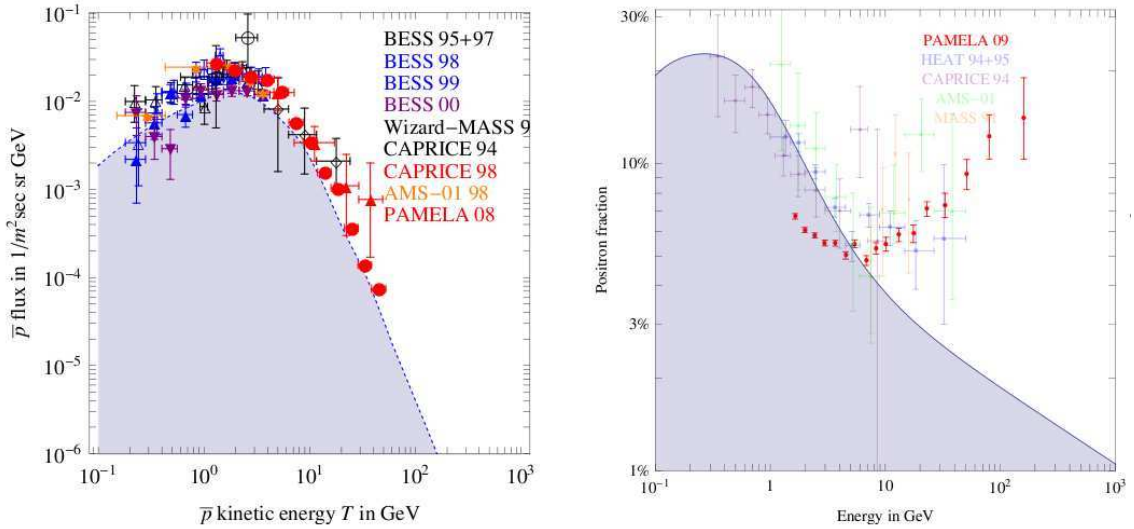

Figure 3.3: Data points of some indirect detection experiments, compared to expected astrophysical backgrounds (shaded grey regions), both for the antiproton and for the positron fraction. Figure taken from [22]

of GeV to TeV, which we are most interested in, photons interact with matter and their interaction length is much shorter than the thickness of the Earth's atmosphere. Anyway quite a lot of ground-based experiments have been developed to observe gamma-rays indirectly, via detecting Cherenkov light and secondary particles originating from their passage through the atmosphere. Among these experiments we find now operating the Cherenkov telescopes HESS, situated in Namibia, and VERITAS, in Arizona, both of them can detect photons up to energies of $\mathcal{O}(100)$ TeV.
Space-based telescopes detect gamma-rays by measuring the properties of e^+e^- pairs produced by their interaction with "conversion foils", usually made by thin sheets of heavy nuclei. The EGRET collaboration has observed photons in a range of energies extending to roughly 30 GeV, the now operating FERMI satellite is instead sensitive to energies of up to several hundred GeV.
Dark Matter is mainly expected to produce gamma-rays by means of showers from its direct annihilation channels, and of the effects of propagation of its charged products in the Galaxy (e.g. via Inverse Compton scattering and Synchrotron radiation). A direct production of photons (e.g. via the channels $\gamma\gamma$ or γZ) is expected to happen only with very small annihilation rates, and then consequent fluxes would be rather difficult to detect. However, that would produce a very high energy "gamma-ray line" (since the mass of DM is thought not to be lower than $\mathcal{O}(10)$ GeV), whose observation would be a clear indication for DM annihilation and for its mass.
Unfortunately till now no such a line has been observed, nevertheless important constraints can be deduced from data of ground-based and space-based telescopes.

However, even unexpected data came from these experiments. In fact, in addition to the photon fluxes, they are able to observe $e^+ + e^-$ fluxes, and here FERMI [26] and HESS [27] agree on the presence of a deviation from the naive power-law spectrum, extending up to energies of $\mathcal{O}(10)$ TeV (see Fig. 3.4). Physicists are trying to explain this deviation and the PAMELA anomaly in a consistent way, by means of Dark Matter annihilations.

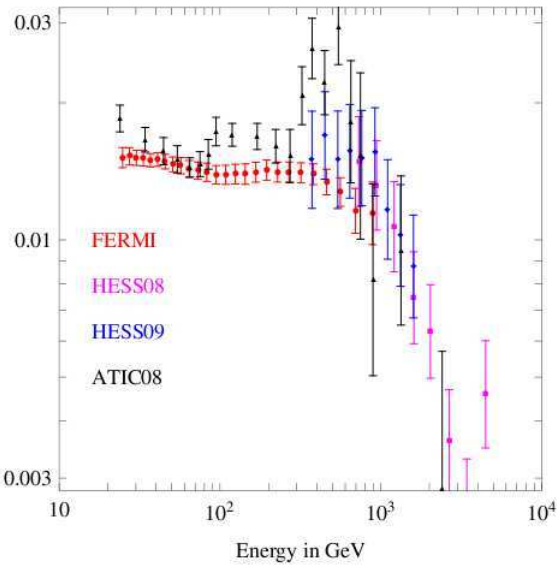

Figure 3.4: Data point of some experiments for the $e^+ + e^-$ fluxes. Figure taken from [22]

To be complete we should mention that, in 2008, the ATIC collaboration found a peak in these spectrum [25], however this result has not been confirmed by most recent observations and is usually not taken into account when trying to give a coherent DM picture of indirect detection experiments.
FERMI and HESS are soon expected to release further more precise data.

3.2.3 Neutrinos

Observation of neutrinos from the sun is also promising for Dark Matter indirect searches. Being the source localised, they can potentially be unambiguous probes of particle Dark Matter models, since detection rates do not depend strongly on the DM halo distribution. The reason why one looks for neutrinos from the sun is rather simple. As WIMPs travel through the universe they scatter off matter and lose in this way small amounts of energy. They can therefore be gathered around large gravitational bodies, increasing their density until their annihilation rate equals half the capture rate (or the whole capture rate for the case of decay). For most of the particle models of DM the two rates are at equilibrium in the sun, from which we then expect a constant flux of neutrinos (the only annihilation product that can escape the sun), on the contrary the same models expect the Earth not

to have reached a similar equilibrium. Of course even neutrinos from the galactic center are important, but, like gamma-rays, they suffer from a high dependence on the DM halo distribution.
Another good aspect of neutrinos is that, with respect to charged particles, the treatment of their propagation is much simpler.
The bad point is that, since they interact weakly with ordinary matter, they're very difficult to detect. The only possibility to do so is by large ground-based experiments, which have to be built underground to keep the backgrounds low. In the $\mathrm{GeV} - \mathrm{TeV}$ energy range neutrinos produce high energy muons via their charged current interaction with ordinary matter, then this muons are detected by the Cherenkov light they emit when travelling through the detector. Examples of neutrino telescopes now active are the Super-Kamiokande, consisting of 50000 tons of water situated underground in the Kamioka mine in Japan, and AMANDA-II, located deep within the ice of the South Pole. Icecube, an improvement of AMANDA-II with a considerably higher sensitivity, is expected to start taking data in summer 2011.
Till now, these experiments have observed no excesses with respect to the expected neutrino fluxes (consisting of atmospheric neutrinos and of neutrinos generated in the interaction of cosmic rays with the sun's corona).

3.3 Implications on particle Dark Matter...

The interpretation of the above experimental situation in terms of Dark Matter does not allow to draw a final conclusion about its nature. Nevertheless, it is useful to predict many of its properties and to exclude or constraint quite a lot of scenarios.

3.3.1 ...from direct detection experiments

We start by exposing the consequences of direct detection experiments:

- *Limits on cross sections*
  The first really important limit imposed by these experiments regards the magnitude of the spin independent interaction cross section of Dark Matter with ordinary matter (see Fig. 3.2)
  $$\sigma_{SI} \lesssim 10^{-41}\, cm^2$$
  It is thanks to this bound that one can assert that Dark Matter is a "weakly interacting massive particle" in a more precise way, in the sense that the only Standard Model interaction allowing for such a small cross section is the weak one. One could observe that the mentioned experiments are actually not probing cross

sections higher than roughly $\mathcal{O}(10^{-30})cm^2$, while the upper limits from astrophysics and cosmology are higher than this value, leaving a window opened in between. As pointed out in [30] an interaction cross section value in this window would lead to a Earth's heat flow much higher than the measured one, so our assertion of DM being strictly weakly interacting is safe.
The limits deduced for the spin-dependent cross section are instead weaker [31]:

$$\sigma_{SD} \lesssim 10^{-35}\, cm^2.$$

- *Vertexes*
  When trying to build a model describing Dark Matter, one cannot evade the requirements of none or very little tree-level interactions with the photon, the gluon and the Z. We already provided reasons for the first two, the third comes from the fact that a vector like interaction with the Z boson would produce a tree level spin-independent elastic cross section of $2 \div 3$ order of magnitudes above the present bounds (see [50] and references therein for further comments and details).

3.3.2 ...from indirect detection experiments

Consequences of Dark Matter interpretation of indirect detection experiments have been widely discussed in literature, here we summarize the model-independent ones (for a complete analysis see e.g. [28] and [29]):

- *Dark Matter mass*
  First of all, a specific requirement for *any* Dark Matter interpretation is indicated by FERMI and HESS data: $e^{\pm}$ spectra from these two experiments become steeper at around 1 TeV, implying the scale of DM mass to be around a TeV.

- *Decay vs. Annihilation*
  Dark Matter fluxes depend on its density ρ_{DM} linearly for the case of decay, and quadratically for the case of annihilation. Then annihilating DM models are more constrained, for example, by the non-observation of a γ excess from the galactic center, while decaying DM models retain a lot more freedom. To be more quantitative, a Dark Matter with a life-time of about

  $$\tau \approx 10^{26}\, s$$

  (10^9 times longer than the age of the universe) could be able to fit all the combined data, of course for particular decay channels.

For annihilating DM the required cross section times velocity is of the order of

$$\langle \sigma_A v \rangle \approx 10^{-23} cm^3/s$$

This value is three orders of magnitudes higher than the one expected from cosmology (2.6). Two physics effects can be taken into account for trying to fill the gap. First, the presence of substructures will change the propagation of particles in the galaxy, resulting in enhancing the cross section by a *boost factor* B. To be sufficient alone, B should be much larger than what suggested by cosmology and/or astrophysics [32], thus another effect is usually considered. Perturbative quantum field theory predicts for the s-wave annihilation cross section (the one that dominates in the non-relativistic interactions which we are considering) a behaviour like $\langle \sigma_A v \rangle \simeq a$, constant in the velocity v. However if the interaction is long range (i.e. the mediator of the interaction is light[1]), a non-perturbative effect, the so-called *Sommerfeld enhancement*, changes the behaviour of the s-wave cross section to $\langle \sigma_A v \rangle \simeq a/v$. To have an intuitive idea, we can think of the classical case of the sun: slower bodies have a larger probability of falling on it by gravitational interaction (i.e a larger cross section), the more interested reader can see [33] and references therein.
Considering these two aspects one can fill the gap between the annihilation cross section suggested by indirect detection experiments and the one predicted by cosmology.
Unluckily, there is no signal that allows one to distinguish between the decaying and the annihilating Dark Matter scenarios in a definitive way.

- *Annihilation/Decay modes*
  Positron together with antiproton fractions data from PAMELA disfavour any non-leptonic final states for DM annihilations or decays, unless $M \gtrsim 10\,\text{TeV}$, moreover leptonic channels are also preferred by FERMI data, since otherwise one would observe an excess in the gamma ray spectrum. Considering then a lot of possible leptonic final states, one can see in a model independent way which of them survive all the constraints given by experiments. It turns out that a 3 TeV Dark Matter annihilating/decaying in 2μ, 4μ or $4e$ is favoured. This is compatible with an interpretation of the data in terms of DM annihilation only for Isothermal halo profiles, while profiles with higher concentrations near the galactic center are safe only in the case of DM decay.

[1]Recently a lot of attention has been paid to models in which DM is charged under a "dark" gauge group, where the new light vector can only decay into the lighter leptons and give rise to large cross sections for four leptons final states. See for example [34].

- *Further data*
  There are some features future data should possess, in order to such an interpretation of cosmic ray excesses in terms of Dark Matter annihilations/decays to be self consistent. First, being M of the order of a TeV, the PAMELA positron fraction should continue to increase over the entire range of energy that PAMELA can explore. Second, FERMI should detect a γ excess due to $e^{\pm}$ inverse Compton scattering on ambient light in the universe, this excess would not be present if the $e^{\pm}$ were generated locally (for example by a pulsar) rather than by Dark Matter in the halo.

Chapter 4

Parton shower algorithms

Monte Carlo programs for the simulation of QCD radiation in high energy scatterings are a fundamental tool in modern particle physics, to the extent that they are integral part of every collider experiment. Not only they are essential for making discoveries, but thay are even necessary in setting up the experiment and in checking its runs.
Due to the important use we will make of them, we give here a quite detailed analysis of the subject. We show how to build the so-called *parton shower algorithm* for the description of multiple radiation in high energy processes involving QCD, this algorithm is the one implemented in the programs mentioned above. We then sketch features about the way they describe hadronization. Finally we expose tha main differences between HERWIG [35] and PYTHIA [36] and conclude.

4.1 Final state radiation

Asymptotic freedom in QCD allows to consider quarks and gluons as free particles in high energy scattering processes involving hadrons.
To describe a process down to lower energies, the hard scattering has to be "dressed" with radiation. It turns out that, to include all the dominant radiation processes, one has to leave the usual fixed order calculation approach: it is in fact suitable for *inclusive* quantities, like total cross sections, while for an *exclusive* description of the final state other tools are needed.

Let us start by considering the simple process $e^+e^- \to q\bar{q}g$.
We ask ourselves which are the kinematical regions giving the dominant contribution to the cross section, with respect to the process without the emission of a gluon. To fix our ideas, let us first consider one of the Feynman graphs appearing in the computation (see

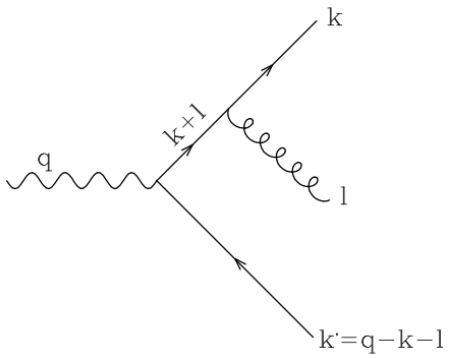

Figure 4.1: Graph contributing to the process $e^+e^- \to q\bar{q}g$

Figure 4.1 for notations). In the amplitude, the propagator yields a factor

$$\frac{1}{(k+l)^2} = \frac{1}{2k \cdot l} = \frac{1}{2\omega E(1-\cos\theta)}$$

where E and ω are respectively the energy of the outcoming quark and photon, and θ is the angle between their spatial impulses.
The factor diverges for *collinear* ($\theta \to 0$) and *soft* ($\omega \to 0$) emissions, we will then be interested in these two dominant kinematical regions.
Note that we have assumed the quarks to be massless, in the following we will always work in this very good approximation (for effects of the quark masses see for example [37, section 3.2]).
For a complete calculation we must take into account both the two graphs contributing to the process (for simplicity we consider the decay of a resonance propagating in the s-channel):

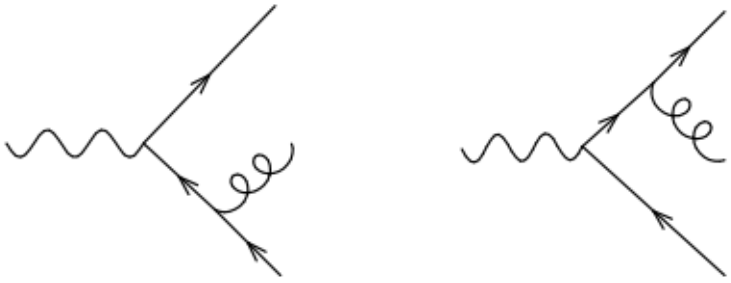

Let k_1, k_2 and k_3 be the four-momenta of the quark, antiquark and gluon, and let q be the four momentum of the resonance. Let x_1, x_2 and x_3 be the ratios of the quark, antiquark and gluon energies to the electron beam energy, $x_i = 2q \cdot k_i/q^2$. They satisfy $0 < x_i < 1$ and $x_1 + x_2 + x_3 = 2$. We introduce also $C_F = (N^2-1)/2N = 4/3$ for the $N = 3$ case, with N number of colours.

We won't be interested in spin correlations, so we mediate over the initial polarizations of the resonance (or spins of the electrons), and sum over the final spins of the quarks and polarization of the gluons, obtaining for the differential cross section $d\sigma$ the result:

$$\frac{d\sigma}{dx_1 dx_2} = \sigma_0 \, C_F \frac{\alpha_S}{2\pi} \frac{x_1^2 + x_2^2}{(1-x_1)(1-x_2)} \tag{4.1}$$

where σ_0 is the Born cross section for the process without the emission of a gluon.
Expression (4.1) is divergent as x_1 or x_2 approaches 1: these singularities correspond exactly to the collinear and soft cinematical regions identified above. In fact $x_1 \to 1$ means that the quark carries away the maximum possible energy, so the antiquark-gluon pair must have a very small invariant mass, corrisponding to configurations in which the two are almost collinear or in which the gluon is very soft (in this last case, $x_2 \to 0$ together with x_1). Similarly, $x_2 \to 1$ means that the quark-gluon pair has a really small invariant mass.

Let us now move to describe the process $e^+e^- \to hadrons$. In order to be complete, we must include in our description subsequent splittings of the partons. This is due to the fact that α_S grows as the energy scale decreases and, with greater importance, that in most quantities of physical interest (like differential distributions), α_S appears multiplied by large logarithmic factors: they have thus to be summed to every order. In doing so we will consider only the contributions coming from the dominant kinematical regions. To fix our ideas, we're going to consider the splitting $q \to qg$, the results obtained can be easily generalized including all the other possible splittings: $\bar{q} \to \bar{q}g$, $g \to gg$ and $g \to q\bar{q}$.

4.1.1 Collinear emissions

In the collinear limit the differential cross section (4.1) assumes the form

$$d\sigma = \sigma_0 \, \frac{\alpha_S}{2\pi} \, P_{qq}(z) dz \, \frac{dt}{t} \tag{4.2}$$

where t is the energy scale of the process and z is the energy fraction carried away by the quark in the limit $t \to 0$. $P_{qq}(z) = C_F \frac{1+z^2}{1-z}$ is the Altarelli-Parisi splitting function of the process, with the notation that the first index is the parton which splits and the second is the one carrying the energy fraction z. Splitting functions of different processes have different behaviours in z, the most notable aspect being that soft singularities emerge only in corrispondence of final state gluons.
The factorization in (4.2) is *universal*, in the sense that it is independent of the process described by σ_0; this property will play a fundamental role in our discussion.
Expression (4.2) holds for different definitions of t, provided that it is proportional to θ^2

in the limit $\theta \to 0$. Common choices for it are the square of the transverse impulse of the gluon with respect to the direction of the splitting particle, the invariant mass of the quark-gluon system, or even the square of the product of θ and the energy E of the quark which splits. Note that t is always taken with the dimensions of the square of an energy. To obtain (4.2) from (4.1) one can proceed as following.
For symmetry, $dx_1\,dx_2 = dx_1\,dx_3$, then, since $x_1 + x_2 + x_3 = 2$:

$$\frac{x_1^2 + x_2^2}{(1-x_1)(1-x_2)} dx_1 dx_2 = \left[-2 + \frac{1 + (1-x_3)^2}{x_3} \left(\frac{1}{1-x_1} + \frac{1}{1-x_2} \right) \right] dx_1 dx_3. \qquad (4.3)$$

Now, in the quark-gluon collinear limit ($\theta \to 0$, e.g. $x_1 \to 1$), it holds

$$1 - z = \frac{x_3}{2 - x_1} \simeq x_3 \quad \text{and} \quad \theta^2 \simeq \frac{4(1-x_1)}{x_3(1-x_3)};$$

finally, since $d\theta^2/\theta^2 = dt/t$, considering the proper Jacobian factor one obtains the desired result.
The above derivation and equation (4.3) put in evidence that, in diagrammatic terms, only the square of the graph containing the collinear partons contributes to (4.2), while the square of the other graph and the interference term are suppressed. This property permits to iterate the universal factorization at each subsequent splitting, provided that they are ordered in t[1]. Then the process of multiple splittings can be described as a Markov chain, in the sense that each splitting is independent of the precedent one. This is summarised in the expression

$$d^{n+1}\sigma = d^{n-1}\sigma \times \frac{\alpha_S}{2\pi} P_{qq}(z') dz' \frac{dt'}{t'} \times \frac{\alpha_S}{2\pi} P_{qq}(z) dz \frac{dt}{t} \theta(t' - t). \qquad (4.4)$$

4.1.2 Soft emissions

The same iterative description can be obtained for splittings with a soft gluon, provided that we order in angle the emissions. In fact in the soft limit the expression (4.1) takes the form

$$d\sigma = \sigma_0 \frac{\alpha_S}{2\pi} \frac{d\omega}{\omega} d\theta\, C_F\, W \frac{d\phi}{2\pi} \qquad (4.5)$$

where ω is the energy of the gluon, ϕ is the azimuthal angle of the gluon with respect to the direction of the splitting quark, and W is the "eikonal factor" (see Figure 4.2 for notations)

$$W = \omega^2 \left(\frac{p}{p \cdot k} - \frac{\bar{p}}{\bar{p} \cdot k} \right)^2$$

[1] note that the energy scale $Q^2 \sim t$ decreases in successive branchings, referring for example to notations of Figure 4.1 it holds $q^2 > (k+l)^2 > k^2, l^2$.

.

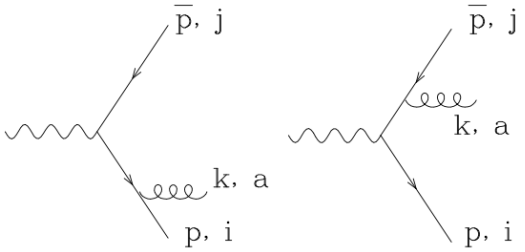

Figure 4.2: Graphs contributing to the emission of a soft gluon

We introduce now $W^{[i]} = \frac{1}{2}\left(W + \frac{1}{1-\cos\theta_{ig}} - \frac{1}{1-\cos\theta_{jg}}\right)$, so that the eikonal fator can be expressed as $W = W^{[i]} + W^{[j]}$, and define ϕ_{ig} as the azimuthal angle of the gluon with respect to the direction of the quark, and θ_{ig} and θ_{jg} as the angles between the direction of the gluon and that of the quark and of the antiquark respectively.
It can be shown that $W^{[i]}$ satisfies (see for example [37, section 5.5])

$$\int_0^{2\pi} \frac{d\phi_{ig}}{2\pi} W^{[i]} = \begin{cases} \dfrac{1}{1-\cos\theta_{ig}} & \text{if } \theta_{ig} < \theta_{ij} \\ 0 & \text{otherwise} \end{cases} \tag{4.6}$$

so after azimuthal integration[2] W becomes the sum of two expressions, one independent of the variables related to the antiquark and the other of the variables related to the quark. Moreover, the behaviour for small θ is exactly the same we found in the collinear limit (4.2), as $1 - \cos\theta \approx \theta^2/2$ for $\theta \to 0$.
We can then interpret each of them as coming from one single graph (see figure (4.2)), and "eliminate" in this way the interference term. This procedure can be iterated, provided that at each step the angle of the emission decreases (*angular ordering*), as required by equation (4.6): the correct choice for the ordering variable t is then any $t \propto E^2\theta^2$. While HERWIG makes this choice, PYTHIA orderes the showers in virtuality (or, as the latest versions, in transverse momentum), with an option to veto branchings that do not fulfill the angular ordering prescription.
Our final iterative result is well illustrated in Figure 4.3.

[2]Note that in the preceding exposition we have always integrated away ϕ, since we were not interested in it.

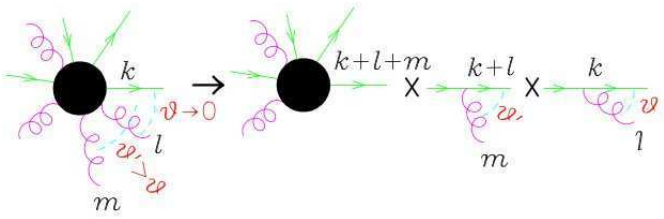

Figure 4.3: Iterative description of multiple emissions

4.1.3 Parton shower algorithm

We are now ready to write the total cross section for the production of n partons:

$$\begin{aligned} \sigma &\approx \sigma_0 \alpha_S^n \int \frac{dt_1}{t_1} ... \frac{dt_n}{t_n} \theta(Q^2 > t_1 > ... > t_n > t_{min}) \int_\varepsilon^{1-\varepsilon} \frac{dz_1}{1-z_1} ... \frac{dz_n}{1-z_n} \\ &= \sigma_0 \alpha_S^n \frac{1}{n!} \log^n \frac{Q^2}{t_{min}} \log^n \frac{1}{\varepsilon} \end{aligned} \tag{4.7}$$

where Q^2 is the initial value of the ordering variable t, taken as the energy scale of the hard scattering $e^+e^- \to q\bar{q}g$.
Expression (4.7) presents divergences in the collinear and soft regions, which have been removed by hand inserting the cut-offs:

- $t_{min} \approx \Lambda^2_{QCD}$ for t, which corresponds to say that at those energies ($\mathcal{O}(1)$ GeV) our perturbative description doesn't hold any more,
- ε, in general t-depending, for z. This cutoff can be justified by saying that the experimental apparatus is not able to measure energies smaller than a certain value, in analogy with the Infrared problem in QED. Different choices for the ordering variable lead to different behaviour of the cutoff in t: for example angular ordering (HERWIG) yields to $\varepsilon \approx \sqrt{t_{min}/t}$, while virtuality ordering (PYTHIA) yields to $\varepsilon \approx t_{min}/t$.

Due to the logarithmic behaviour in the cutoffs, this expression is often referred to as *leading-log approximation*. Subleading terms have lower powers of the two divergent logarithms containing the cutoffs.

These divergences wouldn't have arosen if we had included even the virtual corrections of the same order: the Kinoshita-Lee-Nouamberg theorem assures that such inclusive quantities are free of divergences order by order.

That allows us to write the probability of non emission in the infinitesimal interval dt as[3]

$$P_{NE} = 1 - P_E \simeq 1 - \frac{\alpha_S}{2\pi} \int_{\varepsilon}^{1-\varepsilon} P_{qq}(z) dz \frac{dt}{t}$$

This expression includes, thanks to the 1, all the real unresolved and virtual contributes of the same order.
Let us now divide the finite interval $[t_2, t_1]$ in N small intervals $dt = \frac{t_1 - t_2}{N}$:

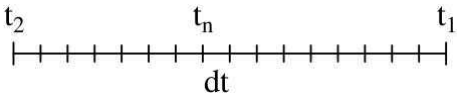

The probability of non emitting radiation as t decreases from t_1 to t_2 is then

$$\begin{aligned} P_{NE}(t_1, t_2) &= \lim_{N \to +\infty} \prod_{n=1}^{N} \left(1 - \frac{dt_n}{t_n} \int_{\varepsilon}^{1-\varepsilon} \frac{\alpha_S(t_n)}{2\pi} P_{qq}(z) dz \right) \\ &= \exp\left(- \int_{t_2}^{t_1} \frac{dt}{t} \int_{\varepsilon}^{1-\varepsilon} \frac{\alpha_S(t)}{2\pi} P_{qq}(z) dz \right) \equiv \Delta(t_1, t_2) \end{aligned}$$

The weight $\Delta(t_1, t_2)$ is called *Sudakov form factor*, it is the "tool" for the description of QCD radiation we were talking about at the beginning of the section: it sums up all dominant virtual and unresolved real emissions to all orders in α_S.
A few other remarks are needed before proceeding:

- Note that $\Delta \to 0$ for $t_2 \ll t_1$, thus the probability that an highly energetic parton doesn't radiate at all downward to the scales of Λ_{QCD} tends to 0.

- It has been proved ([39]) that assuming the transverse momentum at each splitting k_T^2 as the argument of the running coupling constant α_S in Δ allows to sum up a wider class of soft and collinears subleading logarithms.[4]

- Taking into account different types of splitting is straightforward. Each parton species i has its own form factor $\Delta_i(t_1, t_2)$, given by

$$\Delta_i(t_1, t_2) = \exp\left(- \sum_j \int_{t_2}^{t_1} \frac{dt}{t} \int_{\varepsilon}^{1-\varepsilon} \frac{\alpha_S(k_T^2)}{2\pi} P_{ij}(z) dz \right),$$

  where the sum is over all possible processes $i \to j$.

[3] intuitively, $\sigma_{NE} \simeq \sigma_{TOT} - \sigma_{1EM} - \mathcal{O}(\alpha_S^2)$, then we divide by σ_{TOT} and obtain our result, valid for $dt \to 0$.

[4] k_T^2 depends also on z, behaving like $z^2(1-z)^2 t$ for $t \propto E^2\theta^2$.

We are now ready to write the *parton shower algorithm* for the simulation of QCD radiation from a hard process (which fixes the initial energy scale Q^2):

1. For each parton i assign $t_{max} = Q$
2. generate a random number r and solve $r = \Delta(t_{max}, t)$ for t
3. if $t < t_{min}$ the shower stops for the parton "i"
4. if $t > t_{min}$ the splitting $i \to jl$ takes place:
   - generate z from the distribution $\alpha_S(k_T^2)P_{ij}(z)$ (this can be done in practice with the use of the inverse function method)
   - assign $E_j = zE_i$, $E_l = (1-z)E_i$ (then θ_{jl} is fixed)
   - generate ϕ from a uniform distribution
   - restart from point 2., with $t_{max} = t$ separately for the partons j and l.

4.2 Extension to Initial State Radiation

The exposed arguments can be easily extended to the case in which there are hadrons in the initial state.

We work in the *parton model* picture, that is we assume hadrons to be made of elementary constituents, the "partons". Each type of parton "i" is distribuited in the hadron according to the so-called "parton distribution function" $f_i(x)$, where x is the momentum fraction of the hadron carried by the parton (we consider their motion parallel to that of the hadron). The following normalization condition hold: $\sum_i \int_0^1 dx\, x\, f_i(x) = 1$. For simplicity, we're going to consider lepton-hadron scatterings, the generalization to hadron-hadron scatterings is straightforward.

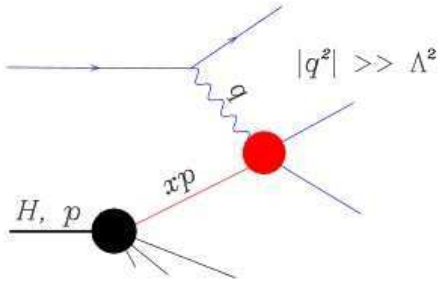

Figure 4.4: Scheme of a lepton-hadron scattering.

We assume that the time scale of the interactions of the partons in the hadron doesn't exceed its inverse mass $1/M_H$, which is analogous to say that the exchanged gluons,

mediators of the strong interaction which keep the partons together, have an energy scale inferior to the hadron mass (otherwise, for the effect of their scattering on other partons, the hadron would "break" into them). We also assume that the momentum transferred from the lepton to the hadron q satisfies the condition $|q^2| \gg M_H^2$, since this is the typical experimental situation (see Figure 4.4).
As a consequence of the above assumptions, we have that the exchanged particle (e.g. a photon) only sees a static snapshot of the p.d.f, and that it scatters on one parton as it were a free particle. It is then reasonable to write, for the lepton-hadron cross section:

$$\sigma(p) = \sum_i \int_0^1 dx\, f_i(x)\, \hat{\sigma}_i(\hat{p} = xp) \tag{4.8}$$

where $\hat{\sigma}_i$ is the cross section for the scattering of the lepton over the single parton i, commonly known as "parton model cross section".

We now want to achieve a treatment of QCD radiation similar to that exposed in the previous section. Since conceptually nothing changes from the description with hadrons only in the final state, we will pass through details and only pay attention to differences with that case.
First of all, we note that collinear and soft singularities won't be removed this time by the inclusion of virtual corrections: for final state radiation this was assured by KLN theorem, that is not the case of initial state radiation, since the theorem holded for inclusive quantities (i.e. a sum over final states was needed). These divergences can nonetheless be removed by reabsorbing them in a scale dependence of the parton distribution functions, $f_i(x) \rightsquigarrow f_i(x,t)$, with $f_i(x,t)$ satisfying the Altarelli-Parisi equations[5], for a detailed presentation see [37, section 5.2] and also [40].
Now we expose the differences of pratical interest in the *parton shower algorithm*.
The first one is that the probability distribution of the first branching is no more uniform in $\Delta(t,t')$, but in $\dfrac{f_i(x_1,t')}{f_i(x_2,t)}\Delta(t,t')$.
The second one is that t is ordered starting from the exchanged momentum q, rather then from the momentum of the initial parton. This "backward evolution" proves much more efficient, since it selects automatically the partons which are going to be involved in the scattering we're interested in; if we had ordered t from the initial momentum only a very small fraction of the partons would have partecipated in the process.

[5]This also turns out to be another way of introducing the Sudakov form factor, moreover in this scheme its generalisation to the case of initial state radiation is easier.

4.3 Hadronization

We have described our process till energies of the order of Λ_{QCD}, at these energies perturbative QCD doesn't hold any more and we need some hadronization model to pass from low energy partons to the observed hadrons. Due to our poor understanding of confinement, this is done in MonteCarlo programs with the use of phenomenological models, which depend on a few non-perturbative parameters to be fixed by best fits to data.
We will now sketch how the models used by HERWIG and PYTHIA work.

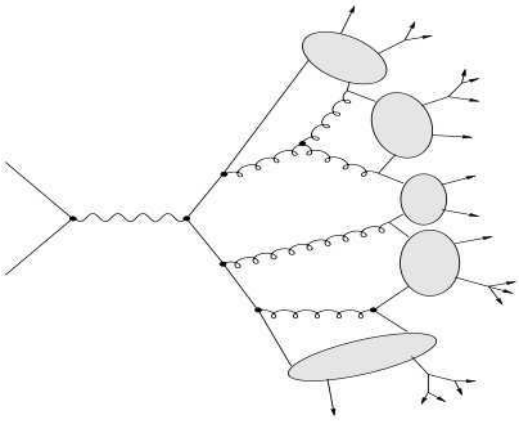

Figure 4.5: HERWIG: cluster model

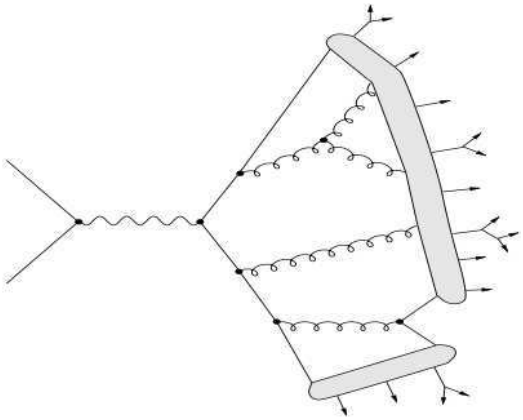

Figure 4.6: PYTHIA: string model

HERWIG uses the so-called *cluster model* [41]: once the parton shower is finished, first it forces all the gluons to split into a quark-antiquark pair, then it collects the nearest quarks which can form a colour-neutral group in a cluster, and finally it parametrically makes the cluster decay into hadrons.
Here a foundamental role is played by colour preconfinement, this property states that colour connected branchings are enhanced by a factor N^2 with respect to other branchings (see [40, section 4.1] for an explicit evaluation), and so partons forming a colour singlet will be near in phase space at the end of the shower.
PYTHIA instead uses the *string model* [42]: it collects all the final partons, even from far phase space regions, in colour neutral strings, then these strings parametrically decay into hadrons. The main point is that colour preconfinement holds only if the shower is ordered in angle, so PYTHIA doesn't expect to find a colour neutral group of partons close in phase space.

4.4 Differences between HERWIG and PYTHIA and conclusions

Till now we've seen that the two programs present differences in:

- the way they order the shower, in angle for HERWIG and in virtuality or in transverse momentum for PYTHIA (with the option to veto branchings not ordered in angle). This doesn't make really big changes, except when comparing with observables sensitive to colour coherence, where HERWIG agrees with data better than PYTHIA,
- the limit of integration in z, given by $\varepsilon \approx t_{min}/t$ for PYTHIA and $\varepsilon \approx \sqrt{t_{min}/t}$ for HERWIG, consistently with virtuality/angular ordering. Here ε is the lower limit of integration, $1-\varepsilon$ the upper one. This leads to a larger z-evolution range in PYTHIA with respect to HERWIG,
- the implemented hadronization models, namely the cluster model (HERWIG), based on colour preconfinement and closely related to angular ordering, and the string model (PYTHIA), both depending on a few non-perturbative parameters.

Other differences we've not seen are:

- the definition of t_{max} in terms of the energy scale of the process Q^2: $t_{max} = 2Q^2$ in HERWIG and $t_{max} = 4Q^2$ in PYTHIA.
- the β function for the running of the coupling constant is included at two-loop level in HERWIG, while in PYTHIA in the one-loop approximation. If we consider for example $\alpha_S(M_Z)$, its actual value comes after fits to LEP data, which yeld $\alpha_S(M_Z) \simeq 0.116$ in HERWIG and $\alpha_S(M_Z) \simeq 0.127$ in PYTHIA. Even if different values of $\alpha_S(M_Z)$ would lead to different total cross sections for hard-scattering processes mediated by the strong interaction, they have very little impact on differential distributions, such as the ones which we are going to investigate, as long as tuned versions of HERWIG and PYTHIA are used.
- the use of different approaches for going beyond the soft and collinear approximations (in the exact matrix element corrections, see [43] for HERWIG and [44] for PYTHIA).

The parameters of the hadronization models, along with other quantities, such as the shower cutoff or quark and gluon effective masses, are fitted to experimental data, like e^+e^- or $p\bar{p}$ data from LEP and Tevatron experiments. In principle, whenever one runs HERWIG or PYTHIA at much higher energies, as will be done in the following, such

fits may have to be reconsidered. In fact when using a hadronization model along with a perturbative calculation or a parton shower algorithm, one assumes that the hadronization model even accounts for the missing perturbative contributions, which are clearly process-dependent. Therefore, whenever one has data from other experiments, one should check that the best-fit parametrizations are still able to reproduce the data.
All that clarifies the importance of the comparison between results of two different Monte Carlo programs, since we will explore energy ranges and processes in which their parameters have not been fitted. In this thesis, for being consistent, we compare results from the default versions of HERWIG and PYTHIA, which were both fitted to LEP data, though keeping in mind that the two Monte Carlo codes may have to be retuned if we were to have in future data which mimic high-mass Dark Matter annihilation.

Extending the algorithm to include photon radiation off quarks and leptons, as well as photon branching into quark or lepton pairs, is straightforward. However, unlike PYTHIA, which includes all such processes, the latest fortran version of HERWIG does not implement photon emissions off leptons as well as $\gamma \to f\bar{f}$ branchings, which are instead present in the latest C++ version HERWIG++[45]. Throughout this work we nonetheless stick to the fortran code.

Chapter 5

Primary Fluxes from HERWIG

As discussed in [28], s-wave non-relativistic DM DM annihilation is equivalent to the decay of a $\mathscr{D}$ resonance with mass $M_{\mathscr{D}} = 2M$. Decays into pairs of Standard Model (SM) particles can be computed in a model-independent way, even taking into account their polarizations, i.e. left- or right-handed fermions, transverse or longitudinal vector bosons. Hereafter we nonetheless neglect polarization issues.
We consider DM annihilations (parameterized by the DM-DM cross section σv) and decays (described by the DM decay rate $\Gamma = 1/\tau$) into the following set of primary SM particles:

$$e^+e^-,\ \mu^+\mu^-,\ \tau^+\tau^-,\ q\bar{q},\ c\bar{c},\ b\bar{b},\ t\bar{t},\ \gamma\gamma,\ gg,\ W^-W^+,\ ZZ,\ hh, \tag{5.1}$$

where $q = u, d, s$ denotes a light quark and h is the Standard Model Higgs boson.
The annihilation into Higgs, gluon and photon pairs deserves further comments.

Since the Higgs boson has not been discovered yet, its mass M_h is obviously unknown: furthermore, the Higgs width and branching ratios strongly depend on M_h, and on the decay modes which are opened for a given M_h. In the following, we will assume that the Higgs mass varies in the range 115 GeV $< M_h <$ 400 GeV; we quote in Table 5.1 the values yielded by HERWIG [35] and PYTHIA [36] for the branching fractions[1]. From Table 5.1, we learn that the branching ratios given by the two programs can differ, especially for low M_h, up to 25% for the decays into vector-boson and $b\bar{b}$ pairs. Such discrepancies are due to the different accuracy which is used to compute the partial widths (see, e.g., [47]). For example, in the decays into WW/ZZ PYTHIA allows both vector bosons to be off-shell, whereas in HERWIG at least one is forced to be on-shell. In the rate of $h \to b\bar{b}$ processes, HERWIG includes also the resummation of mass logarithms $\sim \alpha_S^n(M_h^2)\ln^n(M_h/M_b)$, which are not resummed in PYTHIA.

[1] We recall that SM precision tests favour a light Higgs, $M_h \lesssim 200\,\text{GeV}$, with the LEP2 hint for $M_h \approx 115\,\text{GeV}$ [46].

Higgs mass	Branching ratios in HERWIG (PYTHIA)				qualitative
M_h(GeV)	$W^{(*)}W^{(*)}$	$Z^{(*)}Z^{(*)}$	$b\bar{b}$	$t\bar{t}$	feature
115	6% (8%)	0.7% (0.8%)	81% (73%)	0 (0)	dominant b
135	35% (41%)	4.6% (5.6%)	52% (42%)	0 (0)	mixed W, b
170	96% (96%)	2.5% (2.4%)	1.3% (0.8%)	0 (0)	dominant W
200	74% (74%)	26% (25%)	0.4% (0.2%)	0 (0)	mixed W, Z
300	69% (69%)	31% (31%)	0.1 (0%)	0 (0)	mixed W, Z
400	60% (61%)	28% (29%)	0 (0)	11.2% (10%)	above the t threshold

Table 5.1: *Default branching ratios for the Standard Model Higgs decays in HERWIG and PYTHIA, for a few values of the Higgs mass.*

Final-state γ's deserve special consideration since Dark Matter has no tree-level coupling to photons. Nevertheless $\gamma\gamma$ production can occur at one loop and photons can be emitted by charged particles or produced in three-body decays or radiative hadron decays, such as $\pi^0 \to \gamma\gamma$. To include DM annihilation into three-body final states we would need, however, a specific model of Dark Matter and in this part of the work we prefer to present model-independent results. The case of annihilation into three body final state in a specific model will be the subject of next chapter.

Neglecting the case of coloured Dark Matter, even the DM DM $\to gg$ mode can take place only at one loop. In the Monte Carlo codes employed later on, we implement the $\mathscr{D} \to gg$ decay in the same fashion as $h \to gg$, i.e. with an effective $\mathscr{D}gg$ vertex, and assuming that the two gluons are colour-connected.

5.1 Dark Matter fluxes according to HERWIG

We present the results of the energy spectra of final-state particles from DM annihilation, yielded by HERWIG. For this purpose, we modified the code in order to include the decay of a generic resonance $\mathscr{D} \to ab$, in such a way that the user is allowed to fix the mass $M_{\mathscr{D}} = 2M$ and specify particles a and b. Moreover, we slightly changed the hadron decay tables, to make it sure that hadrons, such as kaons or pions (and even neutrons), which are often treated as stable when simulating collider phenomenology, decay according to the branching ratios quoted in the PDG [48]. Our results will be expressed in terms of the energy fraction

$$x = \frac{K}{M}, \tag{5.2}$$

where K is the kinetic energy of the final-state stable hadrons/leptons/photons in the rest frame of $\mathscr{D}$. We will plot everywhere the particle multiplicity as a function of the logarithmic energy fraction, i.e. $dN/d\log x$; our spectra will be normalized to the average

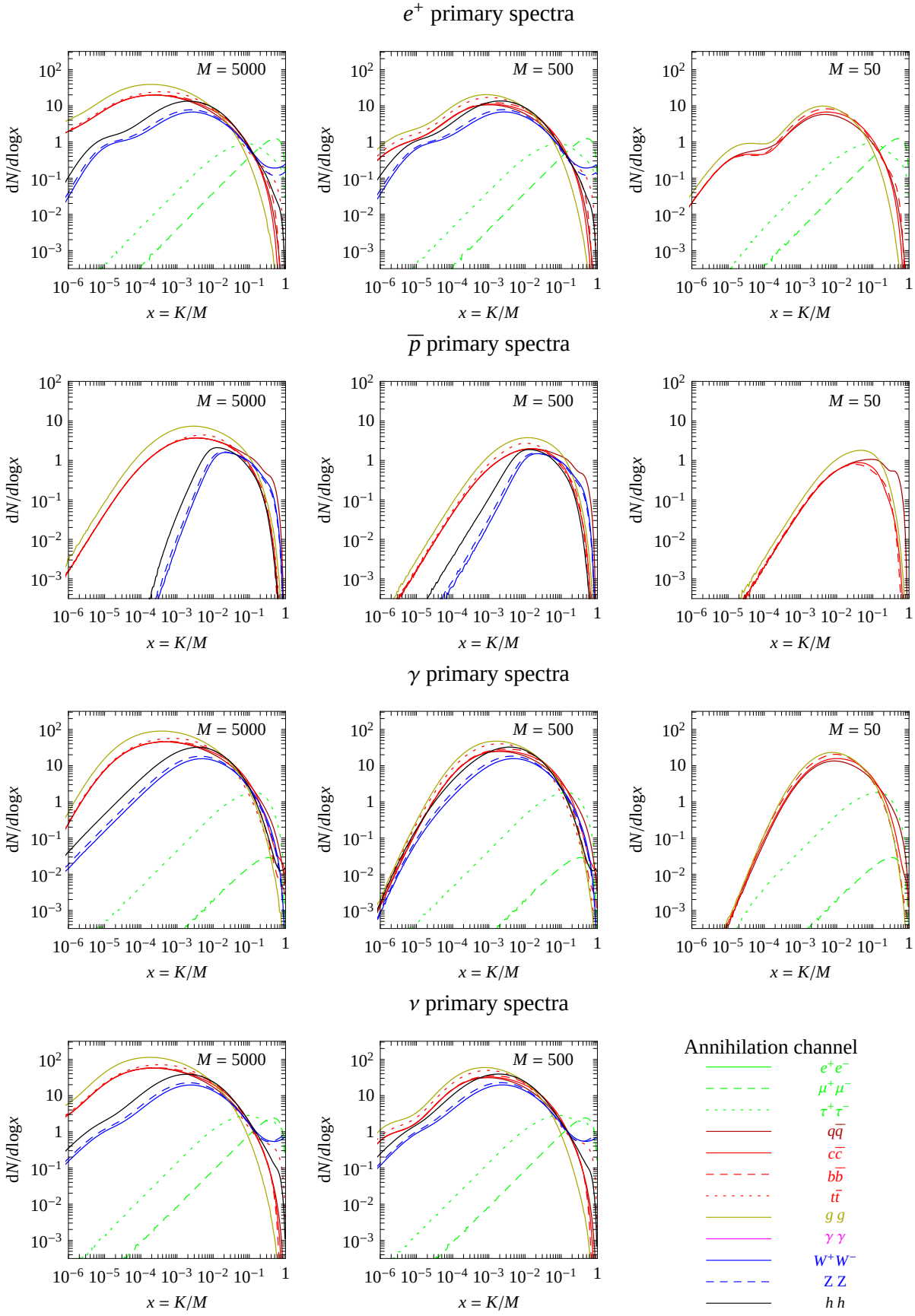

Figure 5.1: Primary fluxes of $e^{\pm}$, $\bar{p}$, γ and $\nu = \nu_e + \nu_\mu + \nu_\tau$. M is expressed in GeV.

multiplicity in the simulated high-statistics event sample (10^7 events).
We computed spectra for the sample of masses $\{50, 100, 500, 1000, 5000, 10000\}$ GeV, however in Figure 5.1 we show plots only for a smaller sample.
An aspect one may remark in the fluxes is the absence of those produced by the e^+e^- and $\gamma\gamma$ annihilation channels. The reason for this fact is that, as we said, the version of HERWIG we used treats final e^+, e^- and γ as stable particles, since it does not include some QED radiation effects in final state showering. So the fluxes yielded by these channels, when present, consist in a very high "line" in $x = 1$ and 0 elsewhere, and then are absent in the event range showed.
Such computing-power demanding results have been obtained using the CIBS cluster of Scuola Normale Superiore.

Having at disposal the energy spectra of charged particles per annihilation at production, as generated by Monte Carlos and as discussed in this section, one would next need to consider where these fluxes of particles are produced in the galactic halo and how they propagate to the Earth. Such an analysis goes beyond the scopes of this thesis, the interested reader is referred to [1] for a discussion, and to [49] for the latest complete treatment of the topic.

5.2 Comparison of fluxes by HERWIG and PYTHIA

An example of the comparison of the DM fluxes from PYTHIA[2] and HERWIG is presented in Figure 5.2, wherein we show the photon, electron, antiproton and neutrino $dN/d\log x$ spectra for the channels DM DM $\to q\bar{q}$, gg, WW and $\tau\tau$.
In Figure 5.2 we have set the DM mass to $M = 1\,\text{TeV}$, but we can anticipate similar $dN/d\log x$ hold for all DM masses $M \gg M_Z, M_t$. Astrophysical experiments are currently probing $K \lesssim 100\,\text{GeV}$, whose corresponding range of x depends on the chosen M; in particular, the low-x tails mostly determine the DM signals if M is very large. Overall, we note the following features:

- For the $q\bar{q}$ modes there is a reasonable agreement between PYTHIA and HERWIG, for all final-state particles and through the whole x spectrum, including the low-energy tails. In fact, although the centre-of-mass energy has been increased to 2 TeV, the $\mathscr{D} \to q\bar{q}$ process is similar to $Z/\gamma^* \to q\bar{q}$ processes at LEP, which were used when tuning the HERWIG and PYTHIA user-defined parameters. Nevertheless, we note some discrepancy, about 20%, especially in the neutrino spectra, as PYTHIA yields overall a higher multiplicity, and in the $\bar{p}$ distribution, where HERWIG is above PYTHIA especially at large x.

[2]for this pourpose we refer to the PYTHIA computation carried out by Mario Kadastik, see [49].

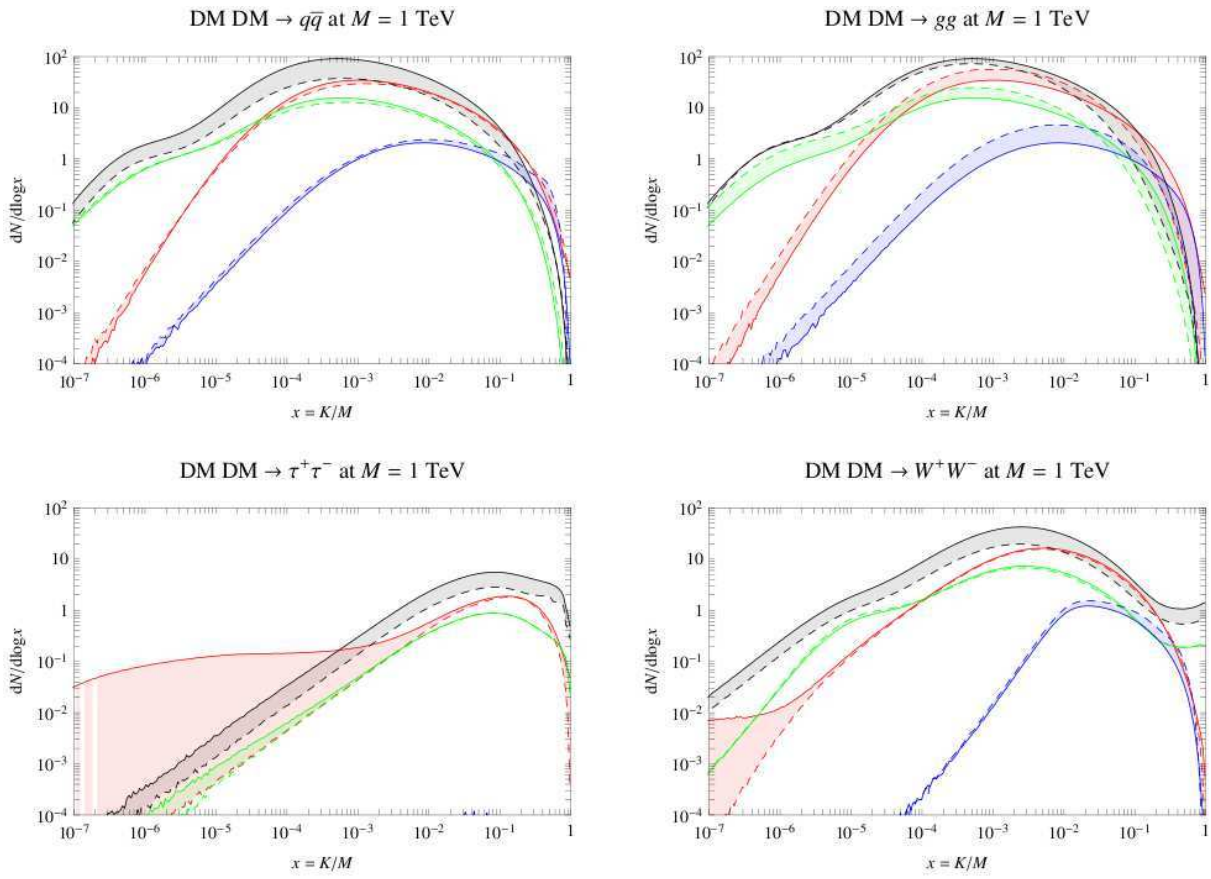

Figure 5.2: PYTHIA is the continuous line, HERWIG is dashed. Photons (red), $e^{\pm}$ (green), $\bar{p}$ (blue), $\nu = \nu_e + \nu_\mu + \nu_\tau$ (black). Figure taken from [49]

- Some disagreement, up to a factor of 2, is instead found for the gg mode, which is presumably not the dominant one, since coloured DM is strongly disfavoured. In fact, unlike the $q\bar{q}$ mode, the $\mathscr{D} \to gg$ channel does not have a counterpart at LEP; the differences in parton showers and hadronization in HERWIG and PYTHIA, as well as the fact that we are running the two codes at a much higher energy with respect to LEP, may thus be responsible of this discrepancy. In detail, as far as the γ, $e^{\pm}$ and $\bar{p}$ spectra are concerned, HERWIG is above PYTHIA at small x and below at large x; the PYTHIA neutrino multiplicity is instead above the HERWIG one in the whole x range, especially for $x > 10^{-5}$.

- Lepton modes (here exemplified by the $\tau^-\tau^+$ case) exhibit a significant disagreement, especially in the photon spectra, where PYTHIA yields a remarkably higher multiplicity with respect to HERWIG for $x < 10^{-2}$. As we pointed out before, PYTHIA includes $\ell \to \ell\gamma$, ℓ being a charged lepton, and $\gamma \to f\bar{f}$ final state processes, which are instead absent in HERWIG, whose photons may come only from $q \to q\gamma$ or radiative hadron decays. The lack of this type of γ radiation in HERWIG

might therefore explain the discrepancy in the photon spectra in the $\tau\tau$ channel.

- The fourth panel shows an example of 'composite' mode, i.e. the DM DM $\to$ W^+W^- channel. This process, wherein a W pair is produced via annihilation of colourless particles, is alike $e^+e^- \to W^+W^-$ at LEP 2, where HERWIG and PYTHIA have been carefully tested. In fact, the electron and positron spectra exhibit good agreement, and even the antiproton multiplicities are not too far, although HERWIG yields a higher $dN/d\log x$ for $x > 10^{-3}$. More visible discrepancies are instead exhibited by the neutrino spectra, as the PYTHIA multiplicity is higher than HERWIG throughout all x range, and by low-x photons, where PYTHIA is much above HERWIG. The latest discrepancy can be traced back to the differences in photon radiation off leptons commented above.

Similar features are observed for other values of the DM mass and for other modes. As we just saw, differences between the spectra yielded by HERWIG and PYTHIA depend on the channel considered, as there are processes/energies the both of them have been tuned to, and others they've not. Overall, keeping in mind the above considerations, we could estimate as 20% the average error given on primary fluxes by Monte Carlo codes.

Chapter 6

Precision check of Electroweak Corrections to the fluxes

Monte Carlo programs include QCD and partly QED effects in their description of high energy scatterings, but they do not implement electroweak (EW) radiation. As we will see, EW radiation has a relevant impact on the spectra of DM annihilation/decay products, thus it is of foundamental importance to include it in computing them. In this chapter we test the precision of a model-independent method of taking into account EW corrections, by means of the comparison with a full computation of the above spectra performed in a specific model (the Minimal Dark Matter model): we will first obtain the exact expressions and then make the comparison.

6.1 The Minimal Dark Matter Model

6.1.1 Invitation

Non-baryonic particles that may fulfill the role of DM have emerged in the last decades within many Beyond the Standard Model (BSM) theories. The most popular one is supersymmetry, but even others, as extra spatial dimension (or Kaluza-Klein) theories, have been widely studied. These constructions try to naturally explain the hierarchy between the electroweak scale and the Planck scale and, in doing so, introduce a host of new particles with EW masses and interactions. Some of these particles can be good DM candidates, for instance the Lightest Supersymmetric particle (LSP) or the Lightest Kaluza-Klein particle (LKP).[1]
However these approaches to the solution of the DM problem, while still the most popular, start facing a sort of "impasse":

[1]For a discussion of these and other candidates, as for a very short introduction to Supersymmetry and Kaluza-Klein theories in light of Dark Matter, see e.g. [1] and [14].

- The expected new physics at the EW scale has not appeared so far at collider experiments: the simplest solutions to the hierarchy problem start needing uncomfortably high fine-tunings of their unknown parameters.

- The presence of a number of unknown parameters (e.g. all sparticle masses) obscures the phenomenology of the DM candidates, for example both the LSP and the LKP vary from model to model.

The Minimal Dark Matter proposal pursues therefore a different and somewhat opposite direction: focusing on the DM problem only, it adds to the SM the minimal amount of new physics (just one extra EW multiplet χ) and searches for the minimal assignments of its quantum numbers (spin, isospin and hypercharge) that make it a good Dark Matter candidate without ruining the positive features of the SM. No ad hoc extra features are introduced: the stability of the successful candidates is guaranteed by the SM gauge symmetry and by renormalizability. Moreover, due to its minimality, the theory is remarkably predictive: no free parameters are present[2] and therefore the phenomenological signatures can be univocally calculated, e.g. at collliders and for direct/indirect detection, up to the astrophysical and cosmological uncertainties.
Another reason of interest for this model is that, being minimal, a lot of more complex BSM theories contain particles which have exactly the same quantum numbers of the MDM succesfull candidates (it is in this sense that the MDM model can be seen as a "scenario"). For instance in most SUSY models the LSP is the lightest neutralino, which is a linear combination of the superpartners of the gauge and Higgs fields. In the region of the parameter space where it is a pure Higgsino, in the range of masses where the annihilation rate into gauge bosons dominate, the lightest neutralino behaves as the fermionic candidate provided by the MDM, (see e.g. [55]).
Therefore studying the MDM model can turn out to be very useful even for other theories which provide successfull DM candidates.

In this chapter we concentrate on the energy spectra dN_f/dx, where we define

$$\frac{dN_f}{dx} \equiv \frac{1}{\sigma_{WW}} \frac{d\sigma_{WWf}}{dx} \tag{6.1}$$

Here x is the energy fraction carried by the particle f, and σ_{WW} and σ_{WWf} are the cross sections for the processes DM DM $\to WW$ and DM DM $\to WWf$ respectively.
The computation of these energy spectra will have two main applications:

- as we said, being a check for the more general topic of systematic inclusion of electroweak radiation in the computation of the fluxes from DM annihilation/decay

[2]This is actually true only for the fermionic candidate, the scalar one has the Yukawa couplings as free parameters

products;

- refining the way experiments constrain some MDM candidates for DM, possibly ruling them out.

6.1.2 Construction

We summarize here the main aspects of the Minimal Dark Matter (MDM) model following a constructive approach, for a detailed treatment see [50], [51] and [52].
The MDM is built by simply adding to the Standard Model a single fermionic or scalar multiplet χ, charged under the usual SM electroweak gauge group $SU_L(2) \times U_Y(1)$, but not under the strong one $SU_c(3)$ (i.e. a WIMP). Its conjugate $\bar{\chi}$ belongs to the same representation (that is, the representation is *real*) and, as a consequence, the theory is anomaly free (see e.g. [38, Chapter 19]).
The Lagrangian of the model is obtained by a "minimal" addition to the SM one:

$$\begin{aligned} \mathscr{L} &= \mathscr{L}_{SM} + \frac{1}{2}\,\bar{\chi}(i\hat{D} + M)\chi \qquad \text{for fermionic } \chi \\ \mathscr{L} &= \mathscr{L}_{SM} + \frac{1}{2}\,(|D_\mu \chi|^2 - M^2|\chi|^2) \qquad \text{for scalar } \chi \end{aligned} \tag{6.2}$$

Here, the covariant derivative D_μ contains the known electroweak gauge couplings to the vector bosons of the SM (Z, $W^\pm$ and γ), and M is a tree level mass term (the only free parameter of the theory). χ is fully determined by its spin and the assignements of its quantum numbers under the gauge group: the number of its $SU(2)_L$ components n and the hypercharge Y.
Starting with all the possible ones, one can see that successful candidates are actually only two: a fermionic quintuplet and a scalar eptaplet. First of all, those with $Y \neq 0$ have vector like interactions with the Z boson, and then, as we saw in Section 3.3, are discarded. This imply that only candidates with even n are possible in order to have null electric charge $Q = Y + T_3$ (where T_3 is the diagonal generator of $SU(2)_L$); moreover it can be shown that fermions (scalars) with $n > 5$ (8) would accelerate too much the running of the $SU(2)_L$ coupling. Finally, imposing stability against decay into SM particles excludes all the possibilities but the two mentioned above [3]. If the condition of minimality is relaxed to include even Yukawa couplings with SM fields, one can see that they actually appear for the scalar eptaplet, but not for the fermionic quintuplet, anyway we won't be interested in this "next-to-minimal" MDM in this work. Therefore, since they have only gauge interactions and null charges Y and Q, both the candidates annihilate at tree level only in W^+W^-.

[3] Strictly speaking even the singlet $n = 1$ survives, but it has no interest because of its total lack of interactions (this is no more the case if full minimality is abandoned).

Assuming that DM arises as a thermal relic in the Early Universe, via the standard freeze-out process, one can compute the abundance Ω_{DM} of MDM as a function of its mass M. Then, requiring that MDM makes all the observed DM measured by cosmology, one can univocally determine M, finding:

$$\begin{aligned} M &= (9.6 \pm 0.2)\,\text{TeV} \quad \text{for the fermionic quintuplet,} \\ M &\simeq 25\,\text{TeV} \quad \text{for the scalar eptaplet} \end{aligned} \tag{6.3}$$

6.2 DM DM $\to W^+W^-\gamma$ and DM DM $\to W^+W^-Z$

Indirect detection experiments provide bounds on the annihilation cross sections of the two MDM dark matter candidates, the most restrictive ones given by the recent HESS photon data [27]. In fact, even varying the DM mass density profile and the model for the propagation of the fluxes in the galaxy, one is not capable to respect these bounds consistently with the value (2.6) for the annihilation cross section $\langle \sigma_A v \rangle$ given by cosmology [29]. This is true even including other effects as the boost factor and the Sommerfeld enhancement, briefly discussed in 3.3.2. So it can be really important to consider the processes where a photon is produced in addition to the two Ws. This has already been done in [51] for the fermionic case, and still the results are not compatible with recent experiments, in the specific sense explained above. One could hope that the same computation carried out for the scalar candidate would change something, unfortunately, as we will see, the expression one obtain for the energy spectra of the γ is (almost) equal to that of the fermionic case.

6.2.1 Fermionic case

Figure 6.1 shows the Feynman graphs that contribute to the process DM DM $\to W^+W^-\gamma$ in the fermionic case. The neutral component of the fermionic quintuplet is the lightest

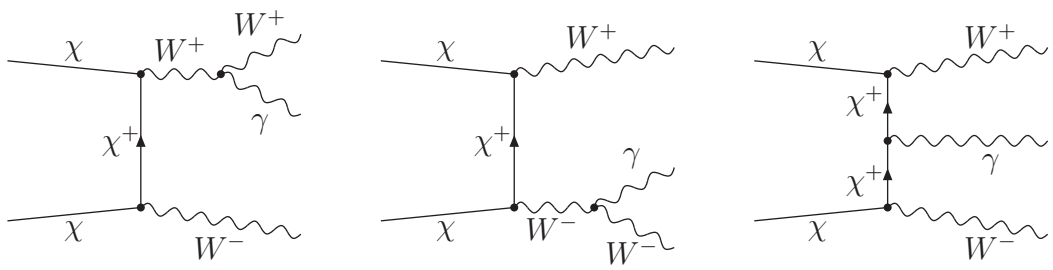

Figure 6.1: Feynman diagrams contributing to the process $\chi\chi \to W^+W^-\gamma$ for fermionic DM. Also crossing fermion lines contribute, but are not shown.

one and it behaves as a Majorana particle, while the other four components are slightly heavier and behave as usual Dirac particles, the mass splitting being a one loop effect of the order $\Delta M \sim 100\,\mathrm{MeV}$ [50, 52]. In the following we can neglect this mass splitting.
As in the preceding chapter we make the well motivated assumption of non-relativistic DM, therefore we perform the computation in the limit of vanishing velocity, i.e. we assume $s = 4M^2$, with M mass of the Dark Matter particle. Moreover we average over initial polarizations and sum over the final ones.
We obtain the full analytical expression for the spectrum dN_γ/dx but, since rather lengthy, we write it defining $\epsilon = M_W/M \ll 1$ and neglecting $\mathcal{O}(\epsilon^2)$ terms:

$$\begin{aligned}\frac{dN_\gamma}{dx} &= \frac{\alpha_{em}}{\pi}\left[\frac{4(1-x-x^2)^2}{x(1-x)}\ln(2/\epsilon) + \right.\\ &+\frac{2(8-24x+42x^2-37x^3+16x^4-3x^5)}{x(1-x)(2-x)^3}\ln(1-x) + \\ &\left.-\frac{2(4-12x+19x^2-22x^3+20x^4-10x^5+2x^6)}{x(1-x)(2-x)^2}\right] \end{aligned} \tag{6.4}$$

Eq. (6.4) agrees with the result computed in [55] for Fermionic DM. We agree with it even in the terms suppressed by $\delta \equiv \Delta M/M_W$, however we do not write them in (6.4) because $\delta/\epsilon \approx \Delta M/M \ll 1$, so their inclusion would require a much higher order expansion in ϵ (in [55] this is not the case since δ and ϵ have not such a precise hierarchy).
Notice that the symmetry $x \leftrightarrow 1-x$ in the first term of Eq. (6.4) reflects that the W bosons can be treated as light ($\epsilon \ll 1$), in fact it tells they have the same infrared behaviour of photons. The kinematical situation where the photon and one of the Ws leave the annihilation point each with maximal energy (and thus there is a very soft W), is enhanced as it would be the one with a very soft photon.

After the substitution $\gamma \rightsquigarrow Z$, the Feynman graphs of Figure 6.1 are exactly those that contribute to the process DM DM $\to WWZ$. Thus computing the spectrum dN_Z/dx at this point is straightforward (of course, keeping in mind the differences such as the sum over final state polarizations and the WWZ vertex). We proceed exactly with the same assumptions and notations we used above for the γ case, and we add the simplification $M_Z \simeq M_W$. As before the full expression is too long to be written here, again we report its Taylor expansion to $\mathcal{O}(\epsilon)$:

$$\begin{aligned}\frac{dN_Z}{dx} &= \frac{\alpha_2}{\pi}\,c_W^2\left[\frac{8-16x+25x^2-18x^3+9x^4}{2x(1-x)}\ln\left(\frac{2x/\epsilon}{\sqrt{1-x+x^2}}\right) + \right.\\ &+\frac{2(8-24x+42x^2-37x^3+16x^4-3x^5)}{x(1-x)(2-x)^3}\ln(1-x) + \\ &\left.-\frac{(52-176x+271x^2-247x^3+150x^4-55x^5+9x^6)x}{2(1-x)(2-x)^2(1-x+x^2)}\right] \end{aligned} \tag{6.5}$$

Again, and for the same reasons explain above, the first term is symmetric under the exchange $x \leftrightarrow 1-x$.

Finally we can easily compute also the relative W spectrum, obtaining:

$$\begin{aligned}\frac{dN_W}{dx} &= \delta(1-x) + \frac{\alpha_2}{\pi} c_W^2 \left[\frac{8-16x+25x^2-18x^3+9x^4}{4x(1-x)} \ln\left(\frac{2x/\epsilon}{\sqrt{1-x+x^2}}\right) + \right. \\ &\quad -\frac{(4-5x+5x^2)}{x^2}\ln(1-x) + \\ &\quad \left. -\frac{80-224x+425x^2-473x^3+341x^4-140x^5+36x^6}{16x(1-x)(1-x+x^2)} \right] + \\ &\quad + \frac{\alpha_{\rm em}}{\pi} \left[\frac{2\left(1-x+x^2\right)^2}{x(1-x)} \ln\left(2x/\epsilon\right) + \right. \\ &\quad -\frac{4-7x+6x^2+x^3-4x^4+2x^5}{x^2(1-x)}\ln(1-x) + \\ &\quad \left. -\frac{30-54x+71x^2-36x^3+12x^4}{6x(1-x)} \right] \end{aligned} \tag{6.6}$$

Here the first term is the leading order annihilation, the one in α_2 arises from 3-body processes with an additional Z, the one in α_{em} from processes with an additional γ.

6.2.2 Scalar case

The Feynman graphs contributing to the process DM DM $\to W^+W^-\gamma$ in the scalar case are shown in Figure 6.2.

As before the neutral component of the multiplet is the lightest one and the mass splitting is a one loop effect of the order $\Delta M \sim 100\,\text{MeV}$, that we neglect. Considering a next-to-minimal scalar eptaplet could yield higher values for the mass splitting (thrugh the Yukawa coupling with the Higgs boson, [50, 52]), however this is not the case in exam.

Again we are interested in the spectra dN_γ/dx, dN_Z/dx and dN_W/dx, as before we compute them assuming $s = 4M^2$ and $M_Z = M_W$.

Incidentally, the analytical expressions we obtain for each spectrum are exactly the same we obtained for the fermionic case. This is true up to $\mathcal{O}(\epsilon^2)$ and/or $\mathcal{O}(\delta^2)$ terms, therefore also for the scalar case we refer to the expressions (6.4), (6.5) and (6.6).

Therefore, since ϵ is very small ($\epsilon \lesssim 10^{-2}$ from the best-fit values (6.3)), the fermionic and the scalar candidates are not expected to give observable differences in the shapes of their energy spectra. As we anticipated in the beginning of the section, this implies that the scalar candidate for DM provided by the MDM model suffers the same problems the fermionic one does.

All the computation in this section have been carried out with the use of the program *Mathematica 7.0*, mainly on the PARC cluster of CERN theory division. These results

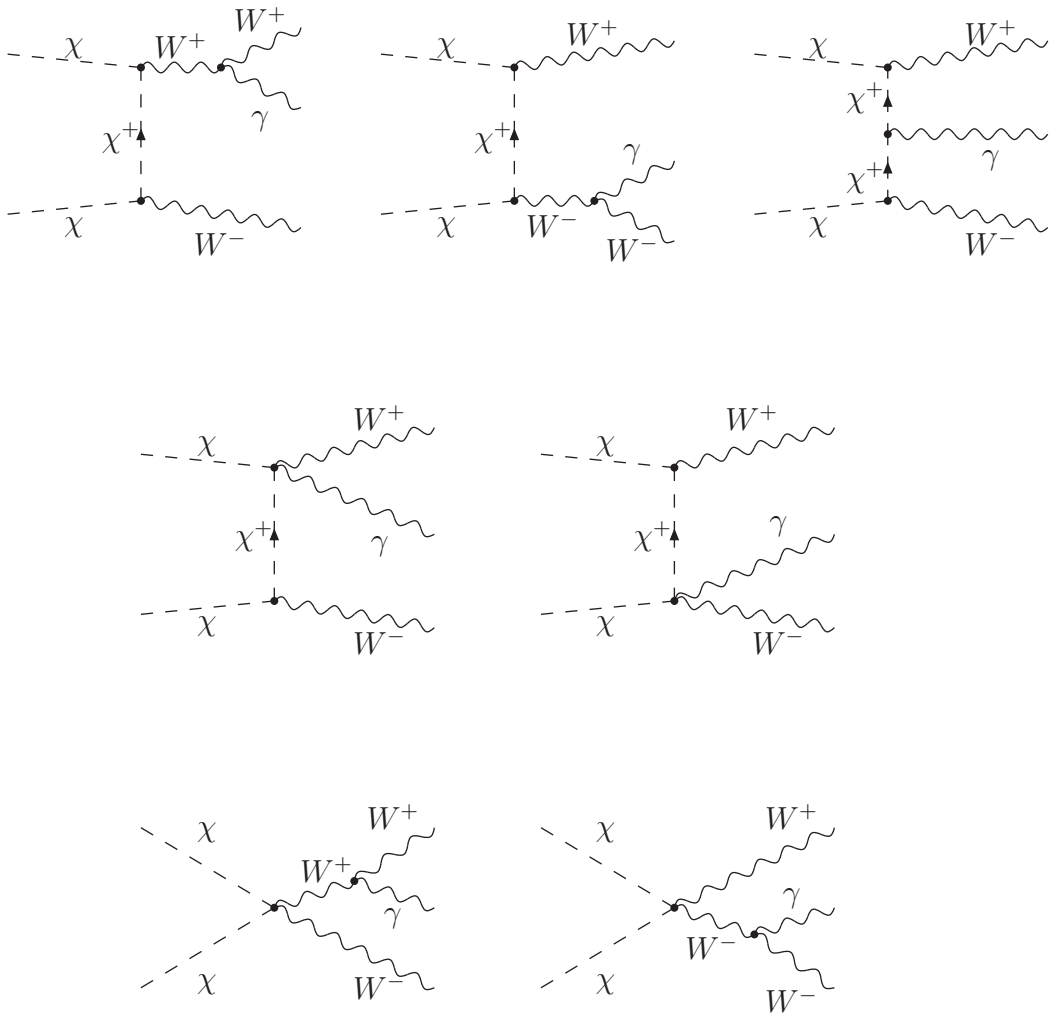

Figure 6.2: Feynman diagrams contributing to the process $\chi\chi \to W^+W^-\gamma$ for scalar DM. For all diagrams with the exception of the last two ones, also crossing scalar lines contribute, but are not shown.

recently appeared in [56].

6.3 Electroweak corrections to DM indirect detection

Electroweak radiative corrections have a sizeable impact on the energy spectra of SM particles originated from the annihilation/decay of DM particles with mass M somehow larger than the electroweak scale. The reason is in fact simple: at energies much higher than the weak scale (in our case the mass M of the DM) soft electroweak gauge bosons are copiously radiated from highly energetic objects (in our case the initial products of the DM annihilation/decay). This is much the same as photon, or gluon, radiation whenever the

hard scale is such that the W, Z masses can be safely taken to be very small. This emission is enhanced by $\ln M^2/M_W^2$ when collinear divergences are present and $\ln^2 M^2/M_W^2$ when both collinear and infrared divergences are present [57], this is known in the literature for both the cases of strong (see 4.1) and weak [62, 58] interactions .
At the typical weak scale of $\mathcal{O}(100)$ GeV, radiative corrections produce relative effects of $\mathcal{O}(0.1)\%$. For instance, this was the case for experiments that took place at the LEP collider. At energies of the order of the TeV scale, like those probed at the LHC, electroweak radiative corrections can reach the $\mathcal{O}(30)\%$ level [59] and they grow with energy, eventually calling for a resumation of higher order effects [60]. Even bearing in mind that weak interactions are not so weak at the TeV scale, one might wonder whether such "strong" electroweak effects are relevant for measurements with uncertainties very far from the precision reachable by ground-based experiments at colliders. It might seem, also in view of our ignorance about the physics responsible for DM cross sections, that these effects should have a minor impact. This is by no means the case: including electroweak corrections has a huge impact on the measured energy spectra from DM decay/annihilation. There are two basic reasons for this rather surprising result.

- In the first place, since energy is conserved, but the total number of particles is not, because of electroweak radiation a small number of highly energetic particles is converted into a great number of low energy particles, thus enhancing the low energy ($\lesssim 100$ GeV) part of the spectrum, which is the one of relevance from the experimental point of view.

- Secondly, and perhaps more importantly: since all SM particles are charged under the $SU(2)_L \otimes \mathrm{U}(1)_Y$ group, including electroweak corrections opens new channels in the final states which otherwise would be forbidden if such corrections are neglected. In other words, since electroweak corrections link all SM particles, all stable particles will be present in the final spectrum, independently of the primary annihilation channel considered.

6.3.1 Summary of EW corrections inclusion

Let us start with an illustrative example: consider a heavy DM annihilation/decay producing an electron-positron pair, see Fig. 6.3. Clearly, as long as one does not take into account weak interactions, only the leptonic channel is active and no antiproton is present in the final products. However the Z radiation opens the hadronic channel: for instance, antiprotons are produced in the Z decay, and also a large numer of pions, which in turn decay to photons ($\pi^0 \to \gamma\gamma$) and to low energy positrons (through the chain $\pi^+ \to \mu^+ + X \to e^+ + X$). At every step, energy is degraded. Because of the large multiplicity in the final states, the total Z energy (already smaller than the hard M scale)

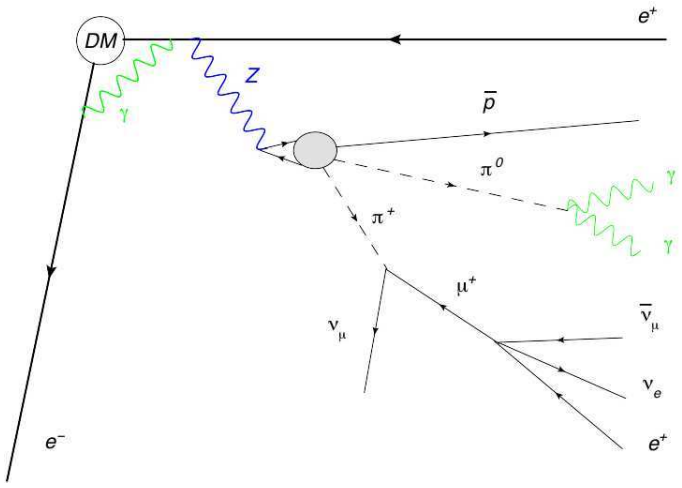

Figure 6.3: *DM annihilation/decay initially produces a hard positron-electron pair. The spectrum of the hard objects is altered by electroweak virtual corrections (green photon line) and real Z emission. The Z decays hadronically through a $q\bar{q}$ pair and produces a great number of much softer objects, among which an antiproton and two pions; the latter cascade decay to softer γs and leptons. Figure taken from [56].*

is distributed among a large number of objects, thus greatly enhancing the signal in the $(10 - 100)$ GeV region that is measured by present-day experiments, like PAMELA.
The various processes of radiation are described by fragmentation functions $D^{\rm EW}(x, \mu^2)$ that evolve with the energy scale μ^2 according to a set of electroweak equations [62]. When a value of virtuality of the order of the weak scale $\mu = M_W$ is reached, the Z boson is on shell and decays. The subsequent QCD showering may be described with QCD traditional Monte Carlo generator tools, like HERWIG.
At tree level, the spectra of hard objects emerging from DM annihilation are simply proportional to $\delta(1 - x)$, where x is the fraction of center-of-mass energy carried by a given particle. Once electroweak corrections are switched on and $\mathcal{O}(\alpha_2)$ virtual and real corrections are calculated, the presence of collinear and/or infrared singularities allows to factorize, in the spectra $D^{\rm EW}(x, \mu^2 = M_W^2)$, leading logarithms (LL) of the form $\alpha_2 \log^2 M^2/M_W^2$ and $\alpha_2 \log M^2/M_W^2$.
These logarithmically enhanced terms can be computed in a model-independent way through the well known partonic techniques based on the collinear approximation. Recently [56] these techniques have been generalized to massive partons. The interested reader is referred to [56] for a detailed discussion of the above techniques, here we only sketch them briefly.

Considering DM that annihilates or decays in one primary channel I, one [56] can obtain a set of basic functions $dN_{I\to f}/dx$ that take into account EW radiation. EW radiation is a model-independent subset of higher order corrections, and gives rise to

specific spectra of initial SM particles, such that its effect can be included in the primary spectra by a convolution with the basic Monte Carlo spectra:

$$\frac{dN_{I\to f}}{d\ln x}(M,x) = \sum_J \int_x^1 dz\, D^{\rm EW}_{I\to J}(z) \frac{dN^{\rm MC}_{J\to f}}{d\ln x}(zM, \frac{x}{z}) \tag{6.7}$$

where $D^{\rm EW}_{I\to J}(z)$ is the EW $I \to J$ *EW parton distribution*: the J spectrum produced by initial I. The indices $I, J = p + \bar{p}$ denote a primary particle p together with its anti-particle $\bar{p}$, with the same energy spectrum.

Similarly to what is done for the well known parton distribution functions in QCD, one can include an energy scale dependence in the $D^{\rm EW}_{I\to J}(z)$, defining $D^{\rm EW}_{I\to J}(z,\mu^2)$ as the probability for a given parent particle I with virtuality of the order of μ to become a particle J with a fraction z of the parent particle's energy. Then one can write for them an evolution equation and solve it at leading order in the EW couplings, taking the tree-level boundary condition $D^{\rm EW}_{I\to J}(x,\mu^2 = s) = \delta_{IJ}\,\delta(1-x)$ (up to re-defining the normalization). The solution can be written in terms of splitting functions $P(z)$, containing the factorized LL terms. These terms can encode the modified kinematics due to the generalization to massive partons, i.e. the fact that the splitting function can be non zero only in the kinematically allowed ranges:

$$\frac{m_f}{E_i} < x < 1 - \frac{m_{f'}}{E_i} \tag{6.8}$$

where $x = E_f/E_i$, and similarly for $x' = 1 - x = E_{f'}/E_i$.

To illustrate these issues and their consequences, consider for example DM producing an initial generic Fermion-anti$F$ermion pair with $F\bar{F}$ invariant mass $\sqrt{s} \gg m_F$. We assume that F has charge q_F under a generic vector V with mass $M_V \ll \sqrt{s}$ and gauge coupling α. (In the SM the vector could e.g. be a Z and the fermion a neutrino). The splitting process $F \to FV$ gives rise to:

$$D_{F\to F}(x) = \delta(1-x)[1+\frac{\alpha q_F^2}{2\pi}P^{\rm vir}_{F\to F}] + \frac{\alpha q_F^2}{2\pi}P_{F\to F}(x), \qquad D_{F\to V}(x) = \frac{\alpha q_F^2}{2\pi}P_{F\to V}(x) \tag{6.9}$$

The first term describes *virtual corrections* arising from one-loop diagrams, and the second term describes real corrections. In the case at hand, we have:

$$P_{F\to F} = \frac{1+x^2}{1-x}L(1-x), \qquad P_{F\to V} = \frac{1+(1-x)^2}{x}L(x) \qquad P^{\rm vir}_{F\to F} = \frac{3}{2}\ell - \frac{1}{2}\ell^2 \tag{6.10}$$

$P_{F\to F}$ and $P_{F\to V}$ contain the universal kinematical function $L(x)$, that holds for massive partons and replaces the usual $\ell = \ln s/M_V^2$:

$$L(x) = \ln\frac{sx^2}{4M_V^2} + 2\,\ln\left(1 + \sqrt{1 - \frac{4M_V^2}{sx^2}}\right). \tag{6.11}$$

This function indeed vanishes below the kinematical threshold ($x < 2M_V/\sqrt{s}$) and reduces to $\ln sx^2/M_V^2$ well above it. This means that *small parton masses, apart from providing kinematical tresholds, give rise to extra* $\ln x$ *factors with respect to the standard case of massless partons*, which become numerically relevant at small x, x'.
Eq. (6.11) has been obtained in [56] by solving the eikonal integral with a specific parametrization of the final impulses, the so-called *exact parametrization*, where x is exactly the energy fraction of the soft final particle. We remember that the eikonal integral is the one that usually appears in the squared amplitudes of three body processes with a soft particle, when integrating over the phase space of that particle (the situation is analogous to the one we saw in 4.1 when introducing the "eikonal factor" W).
What we just saw in a specific example actually holds for all kinds of EW splittings, and is usually known under the name of *improved eikonal approximation*.

6.3.2 Check against our full computation in the MDM

We now see how the above generalization to massive partons improves the usual partonic technique by comparing the both of them to our full computation in the MDM model. The results of the comparison of the Z and γ spectra are shown in Figures 6.4 and 6.5 respectively. Some precisations are in order to understand these figures:

- All the approximated spectra dN/dx have been computed in [56], according to equation (6.7), with $dN^{\mathrm{MC}}_{J\to f}/dx$ obtained with the use of PYTHIA.

- The fundamental factor of the improved eikonal approximation $L(x)$ (6.11) could have been obtained using the *Sudakov parametrization*, the one commonly used to derive similar results for QCD parton evolution. In this parametrization the kinematical end points for the x variable are

$$\frac{M_W}{\sqrt{s}} \leq x \leq 1 - \frac{M_W}{\sqrt{s}}, \tag{6.12}$$

  and the L factor assumes the form:

$$L(x)|_{\mathrm{Sud}} = \ln \frac{sx^2}{M_W^2}. \tag{6.13}$$

We immediately note that, as expected, the usual massless partonic approximation badly fails in reproducing the exact behaviour near the kinematical boundaries, when massive gauge bosons are involved. The improved eikonal approximation shows instead a much better agreement with the exact result, with some differences between the two parametrizations:

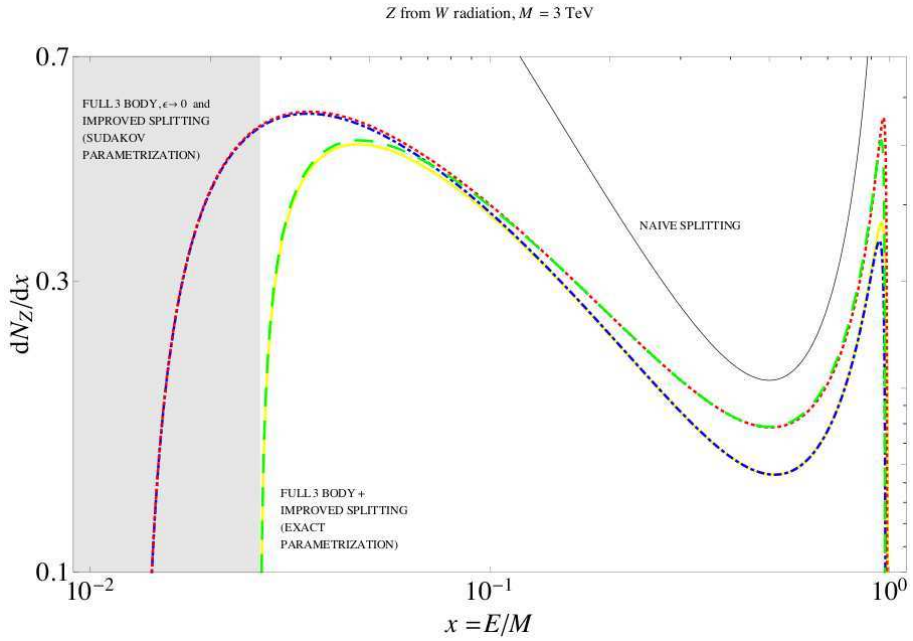

Figure 6.4: Z from W radiation: Comparison between our full result in the Minimal Dark Matter model (continuous yellow line), with its limit for $\epsilon \to 0$ (blue dot dashed) and with the improved eikonal approximation (red dotted for the Sudakov parametrization and green dashed for the exact one). We show also the comparison with the naïve standard partonic approximation (black continuous line). Figure taken from [56].

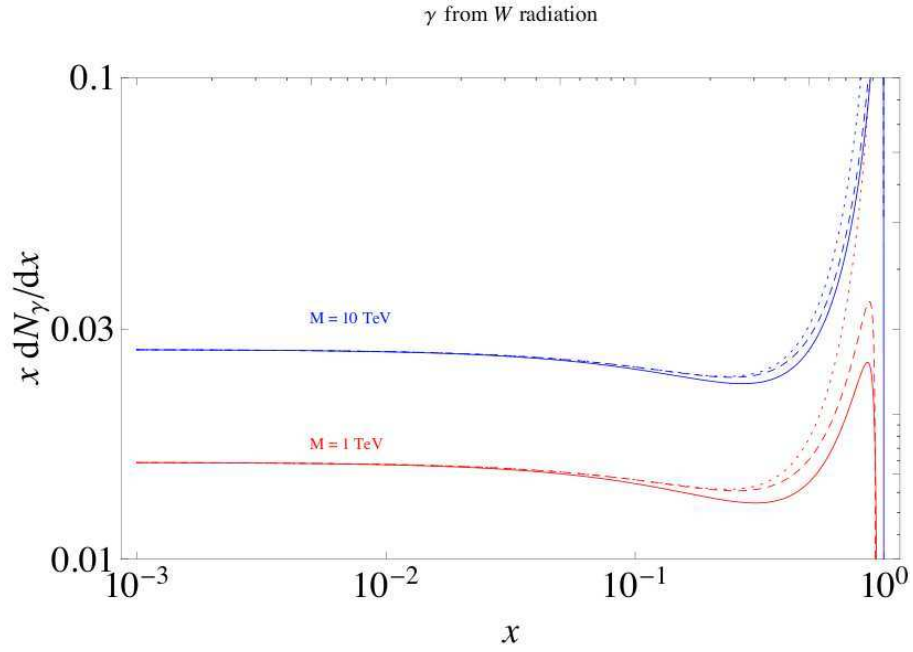

Figure 6.5: γ from W radiation: comparison between our full result (continuous red/blue line) with the improved splitting approximation in the exact parametrization (red/blue dashed) and the standard partonic one (red/blue dotted). Figure taken from [56].

- At small values of x the Sudakov parametrization (red dotted line in Figure 6.4) shows a bad behavior compared with the full calculation[4] and does not respect the correct kinematical end-points:

$$\frac{2M_W}{\sqrt{s}} \leq x \leq 1 - \frac{2M_W}{\sqrt{s}}. \tag{6.14}$$

  This is because in the Sudakov parametrization, considering the splitting process $i \to f + f'$, the variable x doesn't correspond exactly with the fraction of energy carried by the final particle f respect to its initial value, but it does only in the collinear limit (see [56, Appendix B] for details).

- On the contrary the exact parametrization (green dashed line) gives the correct kinematical description of the splitting process and shows a correct agreement with the full calculation.

[4]Notice that its Taylor expansions in ϵ (6.4), (6.5) and (6.6) are only valid at $x \gg \epsilon$, and consequently, like the Sudakov approximation, do not correctly describe the kinematical boundaries.

Chapter 7

Conclusions and prospectives

Indirect Dark Matter searches recently attracted interest because the PAMELA experiment [23] observed an unexpected rise with energy of the $e^+/(e^+ + e^-)$ fraction in cosmic rays, suggesting the existence of a new positron component.
Moreover the FERMI [26] and HESS [27] observations show a deviation from the naive power-law behaviour in the $(e^+ + e^-)$ spectrum, indicating an excess compared to conventional background predictions of cosmic ray fluxes at the Earth. While the current excesses might be either due to a new astrophysical component, such as a nearby pulsar, or to some experimental problem, they could be produced by DM with an appropriate cross section.
In any case, it is undeniable that nowadays indirect search of DM is a fundamental topic in astroparticle physics, both from the theoretical and experimental point of view. Computing the energy spectra of the stable SM particles that are present in cosmic rays and might originate from DM annihilation/decay is therefore of primary importance.

In this thesis we studied radiative corrections to the computation of primary fluxes of of Dark Matter annihilation/decay products. First we did it in a systematic way for a large set of channels and DM masses, using the Monte Carlo program HERWIG. Since Monte Carlo programs differ in the way they implement parton shower and hadronization, and moreover they depend on parameters which are determined by best-fit to experiments, we asked ourselves how much these facts influence the relibility of their previsions for processes they've not been tuned to, like those we want to investigate with Dark Matter Indirect Detection experiments. To answer this question, we compared our results with the same computations performed with PYTHIA over the whole set of DM masses and annihilation/decay channels, and obtained in this way an estimation of the error on the primary fluxes yielded by these Monte Carlo programs. We found that the agreement between the two is quite satisfactory, thus depending on the process considered (better for processes like those used to fit their parameters, worse for the others), the relative discrepancies rarely exceed a 20% value.

It could be useful, in the future, to develop a slighly modified version of HERWIG, including and eventually refining the modifications we made in the code to adapt it to the simulation of DM processes. In this way, the general user working with a particular DM model would be able to easily obtain the relative primary fluxes, starting simply from the various branching ratios given for DM by the model in question. This could find a place into the more general target of developing a tool that, given as input the branching ratios of a particular model, produces as output the stable particles spectra as we see them with direct detection experiments. This tool would of course involve the inclusion of the astrophysical effects on the propagation of primary fluxes, which we have not treated in this work. Today the effort is growing in this direction of simplifying the gap between branching ratios as given by a particular model and observed particle fluxes, see for example [49].

The Monte Carlo programs we dealt with in the first part of the thesis allow to include QCD and some QED radiation effects in the computation of the primary spectra. However, they do not include at all electroweak effects, and even lack in some pure QED processes like the splitting of a gauge boson in the same gauge boson and a photon. Recently, even in light of the LHC experiment start, the inclusion of these EW effects has been widely studied. In fact, they're supposed to become relevant at energies in the TeV scale, inducing corrections that can reach the $\mathcal{O}(30)\%$ level and that grow with energy. Many studies of the most recent results of indirect detection experiments seem to indicate the TeV scale also as the lower bound for the DM mass, thus EW corrections inclusion is worth to be studied even for our pourposes. The importance of EW corrections for DM indirect detection is heightened by the facts that they can even alter qualitatively the spectra, opening new channels in the final state, and that they are expected to affect more the energy ranges currently probed by experiments.
While an implementation in MC codes seems far to be reached, a first order (in the coupling constant) systematic and model independent inclusion of EW effects is possible, in terms of the well-known partonic splitting function formalism. Recently this formalism has been deeply upgraded by its generalization to massive parton through the so-called "improved eikonal approximation", since even the Z and the W are included in EW partons.

In the second part of this thesis we checked the above generalization against a full computation we performed in a specific model. We worked in the Minimal Dark Matter scenario and computed the spectra for the three body annihilations of DM into $WW\gamma$ and into WWZ. We did that for the two succesfull candidates for Dark Matter the MDM offers: a fermionic quintuplet and a scalar eptaplet. By comparing them with the results given by the "improved eikonal approximation" we performed an important test of that technique, finding it in a very good agreement with the exact results. The improvement

with respect to the massless parton technique is evident on the whole energy range, as expected it is striking in the regions where a produced weak gauge boson is soft.
The computations we performed in the MDM model could be useful even for other pourposes: in fact many Beyond the Standard Model theories provide successfull DM candidates which have exactly the same couplings to SM particles that our two MDM candidates have.
The initial reason that induced us to perform the computation was another one: the final spectrum for the γ given by the fermionic DM candidate of the MDM model had already been computed, and was not capable to fit experimental data in a satisfactory way. We wanted to see if this was the case even for the scalar candidate, for which such a computation missed. What we found is that the spectra for the γ do even coincide (when, as in the case of interest, M_W can be neglected), and this feature was confirmed by the Z and the W spectra we computed after.

Experiments to come in the near future, such as IceCube and AMS/02, will keep the attention high on the topics we discussed, and maybe will need a deeper comprehension of the effects of radiative corrections to Dark Matter indirect detection.

Acknowledgements I thank Alessandro Strumia for accepting me as his student despite he was not in Pisa this year. I thank him also for his disponibility and for having introduced me into this stimulating research field.
I thank Gennaro Corcella for his helpful guide when I used HERWIG and for the patient support he gave me whenever any problem arose.
I would also like to thank Marco Cirelli, Paolo Panci, Paolo Ciafaloni and Denis Comelli for very useful discussions.
I thank Scuola Normale Superiore for financial support while at CERN and for all the opportunities given to me in these last two years.

Bibliography

[1] G. Bertone, D. Hooper and J. Silk, Phys. Rept. **405** (2005) 279 [arXiv:hep-ph/0404175].

[2] G. Jungman, M. Kamionkowski and K. Griest, Phys. Rept. **267** (1996) 195 [arXiv:hep-ph/9506380].

[3] J. D. Bekenstein, [arXiv:1001.3876 [astro-ph.CO]].

[4] F. Zwicky, Spectral displacement of extra galactic nebulae, Helv. Phys. Acta. 6, 110-127 (1933) and On the masses of nebulae and clusters of nebulae, Ap.J. 86 217-246 (1937).

[5] M. Roncadelli, "Aspetti Astrofisici della Materia Oscura", Ed. Bibliopolis (collana Saggi scienze filos. natur-Quad.fis.teor), 2004.

[6] D. Clowe, M. Bradac, A. H. Gonzalez, M. Markevitch, S. W. Randall, C. Jones and D. Zaritsky, Astrophys. J. **648** (2006) L109 [arXiv:astro-ph/0608407].

[7] S. Dodelson, "Modern Cosmology" Academic Press, Amsterdam, 2003.

[8] J. F. Navarro, C. S. Frenk and S. D. M. White, Astrophys. J. **462** (1996) 563 [arXiv:astro-ph/9508025].

[9] J. Diemand, B. Moore and J. Stadel, Mon. Not. Roy. Astron. Soc. **353** (2004) 624 [arXiv:astro-ph/0402267].

[10] K. G. Begeman, A. H. Broeils, R. H. Sanders, MNRAS 249, 523 (1991).

[11] J. N. Bahcall and R. M. Soneira, Astrophys. J. Suppl. **44**, 73 (1980).

[12] A. W. Graham, D. Merritt, B. Moore, J. Diemand and B. Terzic, Astron. J. **132** (2006) 2685 [arXiv:astro-ph/0509417].

[13] J. F. Navarro *et al.*, arXiv:0810.1522 [astro-ph].

[14] K. Garrett and G. Duda, [arXiv:1006.2483 [hep-ph]].

[15] S. Gillessen, F. Eisenhauer, S. Trippe, T. Alexander, R. Genzel, F. Martins and T. Ott, Astrophys. J. **692** (2009) 1075 [arXiv:0810.4674 [astro-ph]].

[16] J. Bovy, D. W. Hogg and H. W. Rix, Astrophys. J. **704** (2009) 1704 [arXiv:0907.5423 [astro-ph.GA]]. A. M. Ghez *et al.*, Astrophys. J. **689** (2008) 1044 [arXiv:0808.2870 [astro-ph]].

[17] M. Viel, J. Lesgourgues, M. G. Haehnelt, S. Matarrese and A. Riotto, Phys. Rev. Lett. **97** (2006) 071301 [arXiv:astro-ph/0605706].

[18] M. Viel, J. Lesgourgues, M. G. Haehnelt, S. Matarrese and A. Riotto, Phys. Rev. D **71** (2005) 063534 [arXiv:astro-ph/0501562].

[19] R. Bernabei *et al.*, [arXiv:1007.0595 [astro-ph.CO]].

[20] C. E. Aalseth *et al.* [CoGeNT collaboration], [arXiv:1002.4703 [astro-ph.CO]].

[21] Z. Ahmed *et al.* [The CDMS-II Collaboration], Science **327** (2010) 1619 [arXiv:0912.3592 [astro-ph.CO]].

[22] A. Strumia, "Dark Matter news 2010", talk given at the Planck 2010 conference (2010)

[23] O. Adriani *et al.* [PAMELA Collaboration], Nature **458**, 607 (2009) [arXiv:0810.4995 [astro-ph]].

[24] D. Hooper, P. Blasi and P. D. Serpico, JCAP **0901**, 025 (2009) [arXiv:0810.1527 [astro-ph]].

[25] J. Chang *et al.*, Nature **456** (2008) 362.

[26] A. A. Abdo *et al.* [The Fermi LAT Collaboration], Phys. Rev. Lett. **102**, 181101 (2009) [arXiv:0905.0025 [astro-ph.HE]].

[27] F. Aharonian *et al.* [H.E.S.S. Collaboration], Phys. Rev. Lett. **101**, 261104 (2008) [arXiv:0811.3894 [astro-ph]].

F. Aharonian *et al.* [H.E.S.S. Collaboration], Astron. Astrophys. **508**, 561 (2009) [arXiv:0905.0105 [astro-ph.HE]].

[28] M. Cirelli, M. Kadastik, M. Raidal and A. Strumia, Nucl. Phys. B **813** (2009) 1 [arXiv:0809.2409 [hep-ph]].

[29] P. Meade, M. Papucci, A. Strumia and T. Volansky, Nucl. Phys. B **831** (2010) 178 [arXiv:0905.0480 [hep-ph]].

[30] G. D. Mack, J. F. Beacom and G. Bertone, Phys. Rev. D **76** (2007) 043523 [arXiv:0705.4298 [astro-ph]].

[31] D. S. Akerib *et al.* [CDMS Collaboration], Phys. Rev. D **73** (2006) 011102 [arXiv:astro-ph/0509269].

[32] J. Lavalle, Q. Yuan, D. Maurin and X. J. Bi, [arXiv:0709.3634 [astro-ph]].

[33] J. Hisano, S. Matsumoto, M. M. Nojiri and O. Saito, Phys. Rev. D **71**, 063528 (2005) [arXiv:hep-ph/0412403].

[34] N. Arkani-Hamed, D. P. Finkbeiner, T. R. Slatyer and N. Weiner, Phys. Rev. D **79** (2009) 015014 [arXiv:0810.0713 [hep-ph]].

[35] G. Corcella et al., JHEP 0101 (2001) 010.

[36] T. Sjöstrand, S. Mrenna and P. Skands, JHEP 0605 (2006) 036.

[37] R.K. Ellis, W.J. Stirling and B.R. Webber, "QCD and Collider Physics", Cambridge Univ. Press, UK, 1996.

[38] M.E. Peskin, D.V. Schroeder, "An Introduction to Quantum Field Theory", Westview Press, 1995.

[39] S. Catani, G. Marchesini and B.R. Webber, Nucl. Phys. B 349 (1991) 635.

[40] M.L. Mangano, "Introduction to QCD", in "Lectures, 2008 European school of HEP, Belgium"

[41] B.R. Webber, Nucl. Phys. B 238 (1984) 492.

[42] B. Andersson, G. Gustafson, G. Ingelman, T. Sjöstrand, Phys. Rept. 97 (1983) 31.

[43] G.Corcella and M.H. Seymour, Nucl.Phys.B565:227-244,2000

[44] G.Miu and T.Sjostrand, Phys.Lett.B449:313-320,1999

[45] M. Bahr et al., Eur. Phys. J C 58 (2008) 639.

[46] J. Alcaraz *et al.*, LEP Collaborations and LEP Electroweak Working Group, [arXiv:0712.0929 [hep-ex]].

[47] G. Corcella and D. Rebuzzi, in Proceedings of the Workshop on Monte Carlo's, Physics and Simulations at the LHC PART II', Frascati 2006, [arXiv:0902.0180 [hep-ph]].

[48] C. Amsler et al. (Particle Data Group), Physics Letters B667, 1 (2008) and 2009 partial update for the 2010 edition.

[49] M. Cirelli, G. Corcella, M. Kadastik, P. Panci, F. Sala, A. Strumia, to appear

[50] M. Cirelli, N. Fornengo and A. Strumia, Nucl. Phys. B **753** (2006) 178 [arXiv:hep-ph/0512090].

[51] M. Cirelli, R. Franceschini and A. Strumia, Nucl. Phys. B **800**, 204 (2008) [arXiv:0802.3378 [hep-ph]].

[52] M. Cirelli and A. Strumia, New J. Phys. **11**, 105005 (2009) [arXiv:0903.3381 [hep-ph]].

[53] R. Barbieri, "Ten Lectures on the ElectroWeak Interactions", Edizioni della Normale, 2007. [arXiv:0706.0684 [hep-ph]].

[54] D. Binosi, L. Theubl, Computer Physics Communications 161 (2004) 7686

[55] L. Bergstrom, T. Bringmann, M. Eriksson and M. Gustafsson, Phys. Rev. Lett. **95**, 241301 (2005) [arXiv:hep-ph/0507229].

[56] P. Ciafaloni, D. Comelli, A. Riotto, F. Sala, A. Strumia and A. Urbano, arXiv:1009.0224 [hep-ph].

[57] P. Ciafaloni and D. Comelli, Phys. Lett. B **446**, 278 (1999) [arXiv:hep-ph/9809321].

[58] M. Ciafaloni, P. Ciafaloni and D. Comelli, Phys. Rev. Lett. 84, 4810 (2000); Nucl.Phys. B 589 359 (2000); Phys. Lett. B 501, 216 (2001); Phys. Rev. Lett. 87 (2001) 211802; Nucl. Phys. B 613 (2001) 382; Phys. Rev. Lett. 88, 102001 (2002); JHEP 0805 (2008) 039; P. Ciafaloni, D. Comelli and A. Vergine, JHEP 0407, 039 (2004); M. Ciafaloni, Lect. Notes Phys. 737 (2008) 151; P. Ciafaloni and D. Comelli, JHEP 0511 (2005) 022; JHEP 0609, 055 (2006).

[59] A. Denner, S. Dittmaier and T. Hahn, Phys. Rev. D 56, 117 (1997); A. Denner and T. Hahn, Nucl. Phys. B 525, 27 (1998); M. Beccaria, G. Montagna, F. Piccinini, F. M. Renard and C. Verzegnassi, Phys. Rev. D 58 (1998) 093014; P. Ciafaloni and D. Comelli, Phys. Lett. B 446, 278 (1999); V. S. Fadin, L. N. Lipatov, A. D. Martin and M. Melles, Phys. Rev. D 61 (2000) 094002; P. Ciafaloni, D. Comelli, Phys. Lett. B 476 (2000) 49; J. H. Kuhn, A. A. Penin and V. A. Smirnov, Eur. Phys. J. C 17, 97 (2000); J. H. Kuhn, S. Moch, A. A. Penin, V. A. Smirnov, Nucl. Phys. B 616, 286 (2001) [Erratum-ibid. B 648, 455 (2003)]; M. Melles, Phys. Rept. 375, 219 (2003); J. H. Kuhn, A. Kulesza, S. Pozzorini and M. Schulze, Phys. Lett. B 609 (2005) 277 A. Denner, B. Jantzen and S. Pozzorini, Nucl. Phys. B 761 (2007) 1; J. H. Kuhn, A. Kulesza, S. Pozzorini and M. Schulze, E. Accomando, A. Denner and S. Pozzorini, JHEP 0703 (2007) 078; Nucl. Phys. B 797 (2008) 27; J. y. Chiu,F. Golf, R. Kelley and A. V. Manohar, Phys. Rev. D 77 (2008) 053004; J. y. Chiu, R. Kelley and A. V. Manohar, Phys. Rev. D 78 (2008) 073006; A. Denner, B. Jantzen and S. Pozzorini, JHEP 0811 (2008) 062.

[60] V. S. Fadin, L. N. Lipatov, A. D. Martin and M. Melles, Phys. Rev. D 61 (2000) 094002; P. Ciafaloni, D. Comelli, Phys. Lett. B 476 (2000) 49; J. H. Kuhn, A. A. Penin and V. A. Smirnov, Eur. Phys. J. C 17, 97 (2000); J. H. Kuhn, S. Moch, A. A. Penin, V. A. Smirnov, Nucl. Phys. B 616, 286 (2001) [Erratum-ibid. B 648, 455 (2003)]; M. Melles, Phys. Rept. 375, 219 (2003); J. y. Chiu, F. Golf, R. Kelley and A. V. Manohar, Phys. Rev. D 77 (2008) 053004.

[61] F. Bloch and A. Nordsieck, Phys. Rev. 52 (1937) 54. V. V. Sudakov, Sov. Phys. JETP 3, 65 (1956) [Zh. Eksp. Teor. Fiz. 30, 87 (1956)]. D. R. Yennie, S. C. Frautschi and H. Suura, Annals Phys. 13 (1961) 379.

[62] M. Ciafaloni, P. Ciafaloni and D. Comelli, Phys. Rev. Lett. 88, 102001 (2002); P. Ciafaloni and D. Comelli, JHEP 0511 (2005) 022.